Journal of Volcanology and Geothermal Research

Multi-parametric characterization of explosive activity at Batu Tara Volcano (Flores Sea, Indonesia)

--Manuscript Draft--

Manuscript Number:	VOLGEO_2020_266R1
Article Type:	Research Paper
Keywords:	acoustic signals; Batu Tara volcano; explosive activity; thermal signals; intermediate-size explosions
Corresponding Author:	Laura Spina Istituto Nazionale di Geofisica e Vulcanologia Rome, Italy
First Author:	Laura Spina
Order of Authors:	Laura Spina
	Elisabetta Del Bello
	Tullio Ricci
	Jacopo Taddeucci
	Piergiorgio Scarlato
Abstract:	Batu Tara is an active but poorly studied volcano located in the Lesser Sunda Archipelago (Indonesia). Its last known long-lasting eruptive phase, dating 2006-2015, was characterized by frequent, short-lived explosions, similar in style and magnitude to those of the well monitored Stromboli volcano (Italy). On September 2014, we collected high-frequency multi-parametric measurements of the ongoing explosive activity to investigate the dynamics of intermediate-size volcanic explosions. We acquired synchronised acoustic, thermal and visible high-speed imaging data, and parameterized different spatial and temporal properties of each explosive event: i) maximum height and ejection velocity of bombs and plumes, ii) duration, iii) amplitude of acoustic and thermal transients, iv) acoustic and thermal energy, v) spectral features of the acoustic signals. The latter ones justify the assumption of a pipe resonance of the uppermost conduit section, likely in response to the arrival of over-pressurized gas at the free magma surface. The variability of the investigated parameters agrees with previous observations of intermediate-size explosions at other volcanoes, reflecting the complexity of the related source processes.
Suggested Reviewers:	Jeffrey Johnson JeffreyBJohnson@boisestate.edu Expertize in in the analysis of seismo-acoustic events and intermediate-size explosive activity
	Silvio De Angelis S.De-Angelis@liverpool.ac.uk Expert in the analysis of seismo-acoustic events; has been recently focusing on the acoustic source model theory.
	Letizia Spampinato letizia.spampinato@ingv.it Expert in the investigation of explosive basaltic activity by means of thermal data.
	Matthew Patrick mpatrick@usgs.gov Expert in thermal data and in the analysis of moderate explosive basaltic activity.
	Carolyn Parcheta cparcheta@usgs.gov Expertise in basaltic explosive activity.
Opposed Reviewers:	
Response to Reviewers:	

Multi-parametric characterization of explosive activity at Batu Tara Volcano (Flores Sea, Indonesia)

Laura Spina[1], Elisabetta Del Bello[1], Tullio Ricci[1], Jacopo Taddeucci[1], Piergiorgio Scarlato[1]*

[1] *Istituto Nazionale di Geofisica e Vulcanologia, Sezione di Roma1, Via di Vigna Murata 605, 00143, Rome, Italy.*

**Corresponding author:*

Email: laura.spina@ingv.it

Keywords: explosive activity, acoustic signals, thermal signals, intermediate-size explosions, Batu Tara volcano

Abstract

Batu Tara is an active but poorly studied volcano located in the Lesser Sunda Archipelago (Indonesia). Its last known long-lasting eruptive phase, dating 2006-2015, was characterized by frequent, short-lived explosions, similar in style and magnitude to those of the well monitored Stromboli volcano (Italy). On September 2014, we collected high-frequency multi-parametric measurements of the ongoing explosive activity to investigate the dynamics of intermediate-size volcanic explosions. We acquired synchronised acoustic, thermal and visible high-speed imaging data, and parameterized different spatial and temporal properties of each explosive event: i) maximum height and ejection velocity of bombs and plumes, ii) duration, iii) amplitude of acoustic and thermal transients, iv) acoustic and thermal energy, v) spectral features of the acoustic signals. The latter ones justify the assumption of a pipe resonance of the uppermost conduit section, likely in response to the arrival of over-pressurized gas at the free magma surface. The variability of the investigated parameters agrees with previous observations of intermediate-size explosions at other volcanoes, reflecting the complexity of the related source processes.

1. Introduction

Forecasting the short term progression of volcanic unrest, and defining the physical-chemical processes governing eruptive activity are the main goals of modern volcanology; such objectives require high-quality monitoring data, ideally analysed in near real-time and consistently over long periods (Ebmeier e al., 2019). As such, several volcanoes boast extensive real-time measurements of multiple eruption-related parameters and long-term databases, like Mt. Etna, Vesuvius, and Stromboli (Italy), and Kilauea, Mt. St. Helens, and Yellowstone (U.S.A.) (e.g. Pallister and McNutt, 2015).

Data from volcanoes sited in remote areas are harder to collect, and baselines on their behaviour during unrest are often poor or absent. Not surprisingly, nearly half of the active Holocene volcanoes have rudimentary or no monitoring at all (Ebmeier et al., 2019). Yet the detection and characterization of their eruptive activity have fundamental implications, as even remote volcanoes are not exempt from being a source of possible hazards. For instance, a major risk is posed by volcanic ash to aviation (e.g. Prata and Rose, 2015). The exponential increase of population growth and the sharply increasing air traffic (Tilling, 2008) in the last century stresses the need of mapping the eruptive behaviour of as many volcanoes as possible. Only to quote an example, from 1935 through 2000 about 100 incidents were related to airplanes finding themselves in volcanic ash clouds (Gordeev and Girina, 2014). Additionally, active volcanoes in the vicinity of the sea (either subaerial or submerged) are potentially tsunamigenic (Paris et al., 2014) and might trigger tsunamis through volcano-tectonic earthquakes, slope instabilities, pyroclastic flows, underwater explosions, shock waves and caldera collapse (e.g. Paris et al. 2014; Paris, 2015).

Remote sensing through satellite techniques is a convenient tool to derive near real-time or time-averaged information on the ongoing eruptive activity of remote volcanoes (e.g. Coppola et al., 2019). Nevertheless, the synoptical-scale offered by satellite methods is sometimes not suited to address individual case studies (Pyle et al. 2013), especially considering that the critical spatial resolution for understanding volcanic processes (meter to decametre scale) is uncommon in satellite-based investigation (Ramsay and Harris, 2013). Multi-parametric, *in-situ* observation campaigns, on the opposite, offer a high-resolution robust picture of the eruptive parameters, which is fundamental for understanding the source processes of the eruptive activity (e.g. Dalton et al. 2010; Cimarelli et al. 2016; Spina et al., 2017; Taddeucci et al., 2017, 2021).

Among remote and sporadically monitored volcanoes, Batu Tara (Pulau Komba, Flores Sea, Indonesia) is well known for its analogies with the well-monitored Stromboli volcano in terms of eruptive style and morpho-structural properties (Laiolo et al., 2018). Remarkably, the recent eruptive activity of Batu Tara has posed several concerns for the traffic air, pushing authorities to create alternative commercial routes between Jakarta and Sidney (Sonnabend, 2007). Despite being located on an uninhabited island, its explosive activity threatens the population of nearby islands. In March 2007, 15.000 people were evacuated in response to an increase of the hazard level following a series of stronger explosions. Approximately, 450.000 people reside within 100 km from the volcano, and can be considered exposed to potential risks associated with volcanic activity. Indeed, for Batu Tara, the Population Exposure Index is 2 (out of a maximum of 7; Brown et al 2015). Due to its remoteness, the monitoring of volcanic activity at Batu Tara is mainly realised through i) remote sensing of eruptive plumes (Laiolo et al. 2018; Blackett, 2015), ii) sporadic *in-situ* field observations from Centre of Volcanology and Geological Hazard Mitigation (a.k.a. CVGHM), iii) guided expeditions providing informative reports (Volcano Discovery website; Smithsonian Institution Global Volcanism Program-hereafter GVP- website), iv) and visual observations from Lembata island (CVGHM). Here we describe the results of an extensive characterization of Batu Tara explosive activity through an *in-situ* multi-parametric campaign performed in September 2014 with the aim of drawing a detailed picture of the explosive activity characterizing the volcanic unrest. Using high-quality, high-frequency thermal and acoustic data we i) contributed to the implementation of the baseline knowledge of a scarcely monitored volcano; ii) shed light into the characteristics of intermediate size ash/gas rich volcanic eruptions, a complex end-member of Strombolian and Vulcanian eruptive style.

2. Geological and volcanological setting

Batu Tara volcano is an active stratovolcano located in the Flores Sea (Indonesia), about 46 km north of Lembata Island (Lesser Sunda archipelago). Its steep-sided emerged part forms the isolated and uninhabited 3-km-wide Komba island (4.7 km^2, 748 m a.s.l, 7.792°S, 123.579°E; Blackett, 2015). The base of Batu Tara volcanic edifice lies approximately 3.000 m b.s.l. (Stolz et al., 1988, GEBCO website) while its upper portion is characterised by a lateral collapse scar, very similar to the well-known Sciara del Fuoco in Stromboli volcano, opened to the east and hosting a small active crater (Brouwer, 1940; **Figure 1a**). This morpho-structural analogy, as well as the similar dimensions of their volcanic edifices and persistent explosive activity, have earned Batu Tara and Stromboli the name of “twin volcanoes” (Laiolo et al., 2018).

The magmatism of Batu Tara is linked to the active subduction processes of the 3000 km-long Sunda-Banda volcanic arc system (Hamilton et al., 1979, Van Bergen et al., 1992; Stolz et al. 1988) and is characterised by high-potassium calc-alkaline lavas (Hilton & Craig, 1989). Erupted volcanic products are silica-poor (Stolz et al., 1988; Hoogewerff et al., 1997) potassic to ultrapotassic tephrites, trachybasalt, tephrite basanite, trachyandesite, and basaltic trachy-andesite (Van Bergen et al. 1992, Hilton & Craig, 1989, GVP website, Brouwer, 1940).

The eruptive history of Batu Tara volcano is nearly unknown. Geological evidence at Batu Tara shows that before entering the present explosive cycle, started in 2006, the eruptive style was predominantly effusive, driven by the input of primitive magmas. The transition from predominantly effusive to predominantly explosive activity is attributed to a significantly higher content of volatiles retrieved in recent magmas (Herrin and Costa, 2015). The only documented eruptive phase pre-2006, characterised by explosions and lava flows, dates back to the period 1847-1852 (VEI-2; Stolz et al., 1988) although some sources extend this eruptive period up to 1932 (Brouwer 1940; Badan Geologi Website).

The present-day activity of Batu Tara initiated on 1 July 2006, when an ash cloud was reported (VEI-1; GVP website, 2007), interrupting an over a century-long period of dormancy. In the period 2007 – 2015, the activity was characterised by the persistent occurrence of Strombolian to Vulcanian explosions emitting gas, ash and ballistic blocks in variable proportions, and was documented by: i) the Darwin Volcanic Ash Advisory

Centre, who issued a total of 2652 advisories for Batu Tara (Volcanic Ash Advisories: 4 in 2006, 134 in 2007, 251 in 2008, 532 in 2009, 380 in 2010, 348 in 2011, 482 in 2012, 333 in 2013 with an archive gap for December 2013, 90 in 2014, and 98 in 2015; source VAAC Darwin Archive), and ii) thermal anomalies detected by the Moderate Resolution Imaging Spectroradiometer (MODIS) on NASA's Terra satellite from Hawai'i Institute of Geophysics and Planetology (MODIS website). A continuous ash emission characterised the beginning of this eruptive phase, then the activity shifted toward frequent (i.e. several per hour) ash-rich Strombolian explosions and more energetic Vulcanian-type explosions occurring several times per day. These latter ones ejected bombs and blocks up to 500 meters above the crater. On 24 March 2007, a series of stronger eruptions (VEI-2) forced Indonesian authorities to raise the alert level to 3 (out of a maximum of 4) and evacuate 15,000 people from Lembata Island, 50 km to the south (Volcano Discovery website, Volcano Live website). The alert level was then lowered to level 2 on 12 April 2007 (GVP website, 2007). On 5 April a lava flow on the eastern slope created a lava delta 450 m across and extending 100 m offshore (GVP website, 2007). In 2015, explosive activity waned, followed by only rare MODIS thermal anomalies detection, the last of which on 16 July 2016 (MIROVA Team pers. comm.; methodology in Coppola et al., 2015).

During the above-described period, and the period investigated in this work, the explosive activity was ejecting ash, and lapilli- to bomb-sized pyroclasts, with some ash plumes reported by the Darwin VAAC reaching as high as ~ 3 km a.s.l. and drifting laterally up to 200 km from Batu Tara. A small pyroclastic flow was observed on 3 July 2015 travelling down the eastern scar and for about 250 m out to sea (GVP website, 2016; Volcano Discovery website).

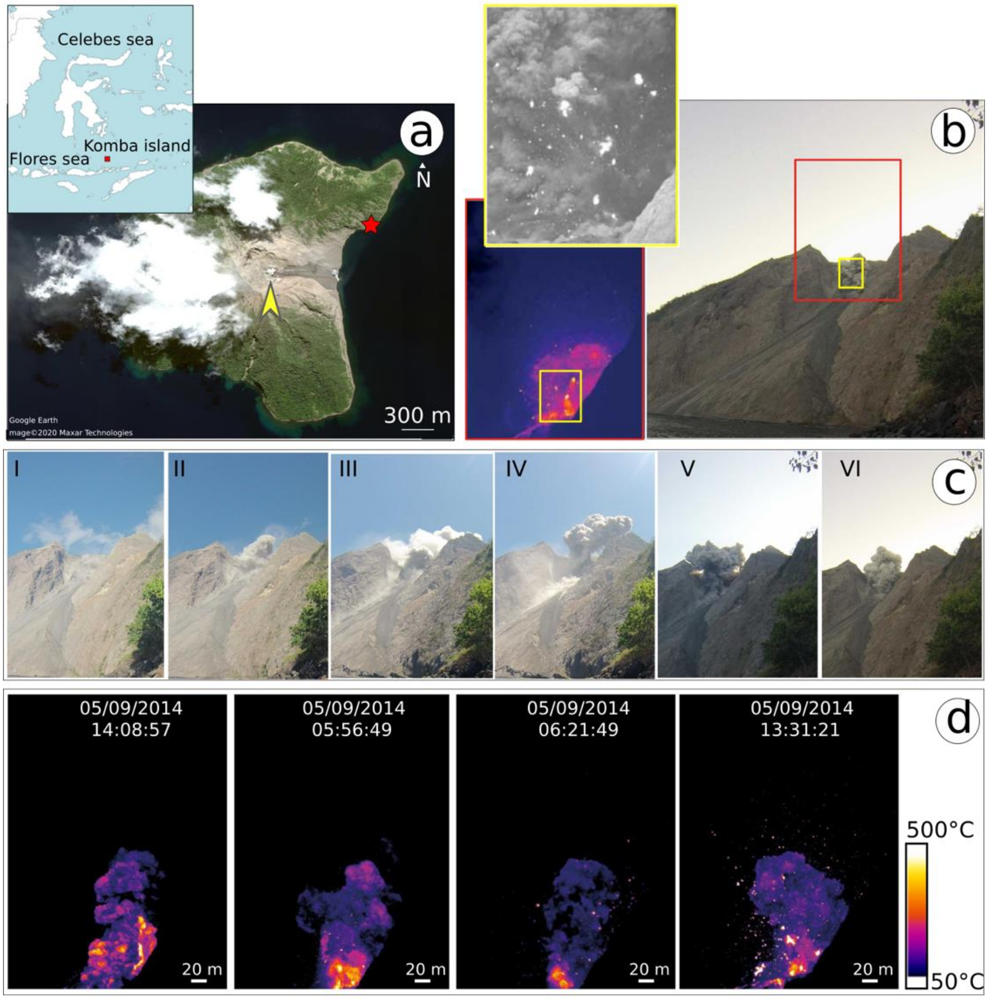

Figure 1: (a) Geographical position (top-left inset), and aerial view (2012; Image ©Maxar Technologies) of Komba Island. The active vent of Batu Tara is marked by a yellow arrow, below a small eruptive cloud. The position of the multi-parametric setup is marked by a red star. The distance between the recording site and the active vent is 1226 m. (b) Picture of Batu Tara volcano showing the field of view of the camera (FOV). Thermal (bottom left inset) and visible (top left inset) camera images with horizontal FOV of 244 m and 60 m, respectively. (c) Snapshots from different eruptive events recorded by a GoPro camera corresponding to the acoustic events in Figure 3 marked by an event serial number of 3 (I,05/09/14 00:28), 11 (II, 05/09/14 01:47), 17 (III, 05/09/14 04:44), 18 (IV, 05/09/2014 04:56), 31 (V, 05/09/14, 10:12), 33 (VI, 05/09/14 11:00). (d) Still frames of four selected explosions as recorded by the FLIR thermal camera (FOV 244x346m), showing the observed events ranging from ash-dominated explosions (left) to bomb-dominated explosions (right).

3. Field deployment

The field campaign at Batu Tara was performed from 4 to 6 September 2014. Multiple, time-synchronized devices were deployed at sea level in direct view of the active vent, which was located at a straight distance of 1226 m and at an elevation of 540 m a.s.l. The multiparametric setup included: i) a high-speed camera (OPTRONIS CR600x2, recording at 500 frames per second (fps) with a pixel size of 0.06 m) acquiring videos of the vent in the first 20 seconds of explosions; ii) a thermal infrared camera (FLIR SC655 , 50-200 fps, pixel size of 0.51 m), acquiring videos at a larger spatial and temporal scale; iii) a time-lapse camera (GO-PRO, 1 frame every 5 s) (**Figure 1b**), and iv) a broadband microphone (freq. range of kHz to 0.1 Hz) sampled at 10 kHz. The multi-parametric station recorded discontinuously several seconds- to minutes-long traces each one comprising one or two explosive events. In this study, we primarily focus on the integrated analyses of thermal and acoustic data, since these two datasets captured the whole explosion dynamics for a large number of events at a comparable spatial/temporal resolution. High-speed videos are here used to obtain quantitative constraints on the vent geometry and exit velocity as detailed in **Section 4.1**.

During the recorded period, the activity was characterized by impulsive, ash-rich explosions lasting seconds to minutes. The explosions ejected ash-loaded jets, with variable proportions of hot lapilli- to bomb-sized pyroclasts and spatters 100-300 m above the crater, that eventually fell/rolled down the eastern collapse scar. The ash was rapidly dispersed buoyantly in small plumes rising up to a few hundred meters above the vent before being drifted away by local wind (**Figure 1c**). The activity spanned from pure ash venting with negligible amounts of incandescent material to bomb-dominated explosions (**Figure 1d**). Rarer, significantly more powerful blasts were also observed ejecting meter-sized blocks to distances of several hundred meters in all directions.

4. Data analysis

4.1 Thermal infrared video analysis

Thermal videos captured several explosions with a horizontal field of view ranging from 61 to 244 m in width and up to ca 350 m above the vent (bottom inset in **Figure 1b** and **Figure 1d**). The vent was not directly visible from our point of observation. However, using high speed and thermal images of different events, we estimated the horizontal width of the jet just above the crater rim at the very beginning of the explosions to be in the range 6 - 20 m, suggesting that the eruptive vent might have a similar size at its exit. Thermal images were corrected for the atmospheric absorption through the software after air temperature, humidity, and target distance input, and then scaled by knowing pixel pitch size (17µm), lens focal length (41.3 mm), straight distance (1226 m), and dip angle of the camera (20°). Quantitative analysis of the thermal infrared videos was carried out by using different image processing in-house-built algorithms.

In a first approach, for each video frame we integrated the apparent brightness temperature of all pixels in a 100x50 pixel control area (A) above the vent and subtracted the background temperature, i.e. the minimum temperature of each frame; then, dividing by A we obtained a mean temperature value representative of the whole frame. Variations of this value over the different frames of the video provides thermal signal variation over time, or the 'thermal waveform' (**Figure 2**). In this way, each explosion, characterised by a single thermal pulse or by a sequence of two or more pulses, can be quantitatively detected from the thermal waveform analysis, after de-trending and de-meaning the signal, by using a Short Time Average/ Long Time Average (STA/LTA) algorithm (Withers et al., 1998), and using STA window = 1 s, LTA window 40 s, trigger threshold STA/LTA=3, de-trigger threshold STA/LTA=1). Moreover, we estimated the thermal energy radiated from each explosion according to the Stefan–Boltzmann Law, by integrating the radiant flux emitted in the control area (A) over time (t) (Bombrun et al., 2016, Marchetti et al., 2009) as follows:

$$E_{th} = \int_{t_i}^{t_f} \int_A \sigma\varepsilon(T^4 - T_0^4)dA\, dt \quad (1)$$

where t_i and t_f are the initial and final times of the event obtained from the STA/LTA detection (and t_f–t_i being the event duration), ε is the emissivity of the surface (assumed constant, 0.96), σ is the Stefan-Boltzmann constant (5.670373×10^{-8} Wm^{-2} K^{-4}), and T and T_0 the pixel and the ambient environment temperature (K). From this analysis, 67 out of 72 detected vents were selected.

In a second approach, we used a Matlab algorithm (Gaudin et al., 2017) to discriminate the dynamics of each explosion as a function of time as follows: for each frame in a video, the maximum temperature (T_{max}) value is computed for each row after the background temperature (T_b) is subtracted considering the minimum temperature of each pixel in a 2-second moving time-window preceding the frame. In this way, the quantity

(T_{max}-T_b) of each frame row is represented graphically as a function of height above the vent (in the y axis), and time (on the x axis) allowing to visualize the time evolution of the temperature anomaly generated by the erupted material (**Figure 2**). In these 'rise diagrams' hot gas and ash and bombs appear as blurred stripes and well-defined parabolic curves, respectively, with an inclination proportional to their rise velocity. From these diagrams, we retrieved manually the following quantities: i) explosion starting time, ii) maximum bomb elevation, and iii) maximum plume elevation, from which we computed their maximum height and mean rise velocity.

Using the rise diagrams and high-speed video footage we assessed semi-quantitatively the bomb content of the events, attributing a 'bomb-index value' ranging from zero for ash-dominated, bomb-free explosions to one for bomb-dominated explosions (**Figure 1d**).

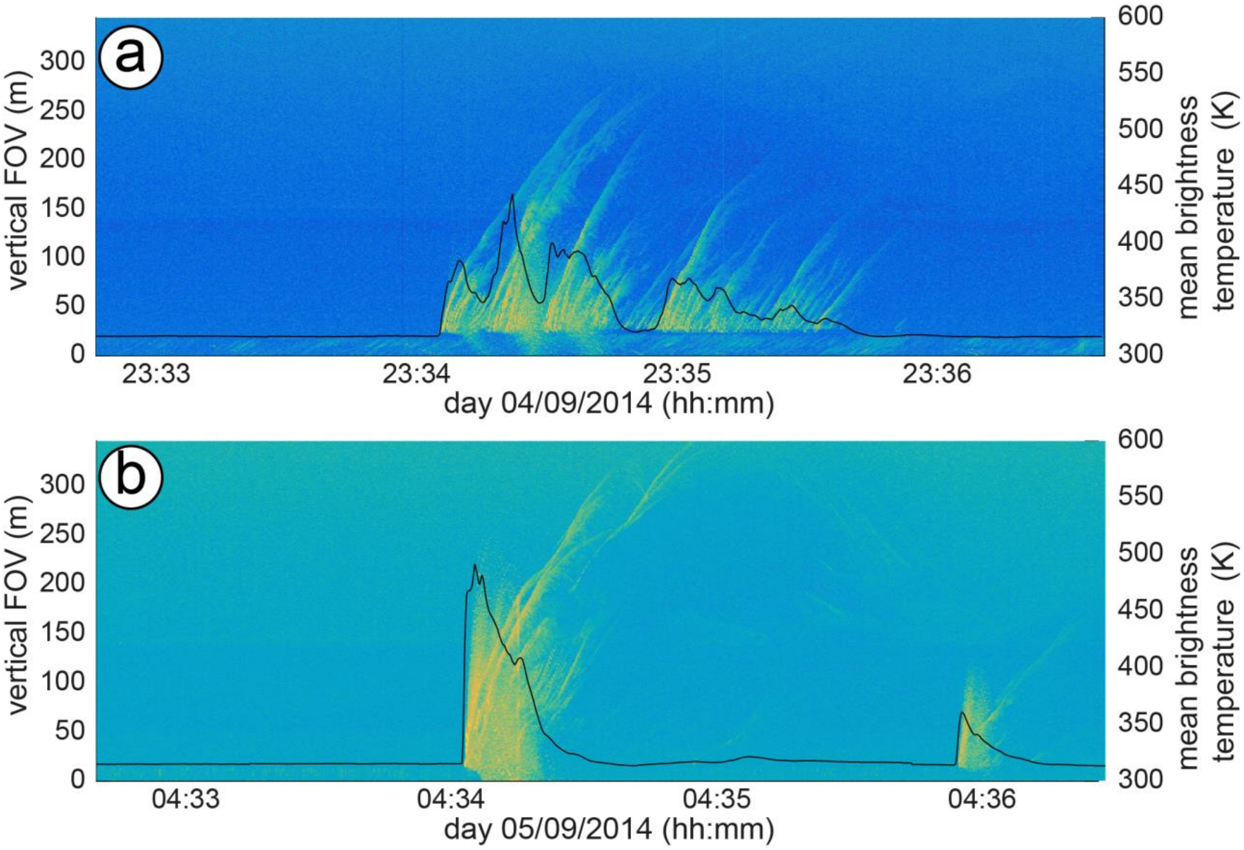

Figure 2: Two examples of explosive events of Batu Tara represented after processing the high-frequency thermal videos. In each plot, on the left y-axis we diagram time vs height variation of the temperature

anomaly generated by the explosive event, or 'rise diagram', whereas on the right y-axis, we plot the average brightness temperature in a control area, or 'thermal waveform'. The thermal anomaly is the maximum temperature computed for each row of thermal image after background subtraction (T_{max}-$T_{b,}$ color-coded). Gas puffs and bombs appear as streaks and parabolas, respectively, with a slope related to their rise (or fall) velocity. The thermal waveform is calculated as the frame-by-frame sum, after background subtraction of T values in a 100x50-pixel box above the vent. This quantity is superimposed in the previous diagram, showing that events are characterised by an initial jet phase, followed by the one or more bursting pulses, and a final waning phase.

4.2 Acoustic signal analysis

Acoustic signals were decimated to 100 Hz to improve processing speed. The decimation does not affect signal properties, given that the bulk of energy content of Batu Tara explosions lies in the infrasound range. To pick acoustic transients from the data, we applied the STA/LTA algorithm using a short-time window and a long-time window, a trigger and a de-trigger threshold of respectively 1 and 5 seconds, 4 and 1.5. Such parameters have been broadly texted to maximize the detection capability of the algorithm.

Accordingly, 72 acoustic transients with good signal to noise ratio have been selected (**Figure 3**) and characterised using different parameters. Event duration was computed as the time interval between trigger and de-trigger thresholds. Spectral and time-domain properties of the events were computed on a window of 10.24 seconds. In particular, we evaluated the peak-to-peak and Root Mean Square (RMS) amplitude of the events and their peak frequency. We additionally computed a parameter that account for the contribution of higher frequencies to the spectrum, the mean frequency f_{mean}:

$$f_{mean} = \frac{\sum_{i=1}^{N} (pxx_i * f_i)}{\sum_{i=1}^{N} pxx_i} \quad (2)$$

with pxx_i corresponding to the power spectral density evaluated at each of the N frequencies f_i (Carniel et al., 2005; Spina et al., 2016a).

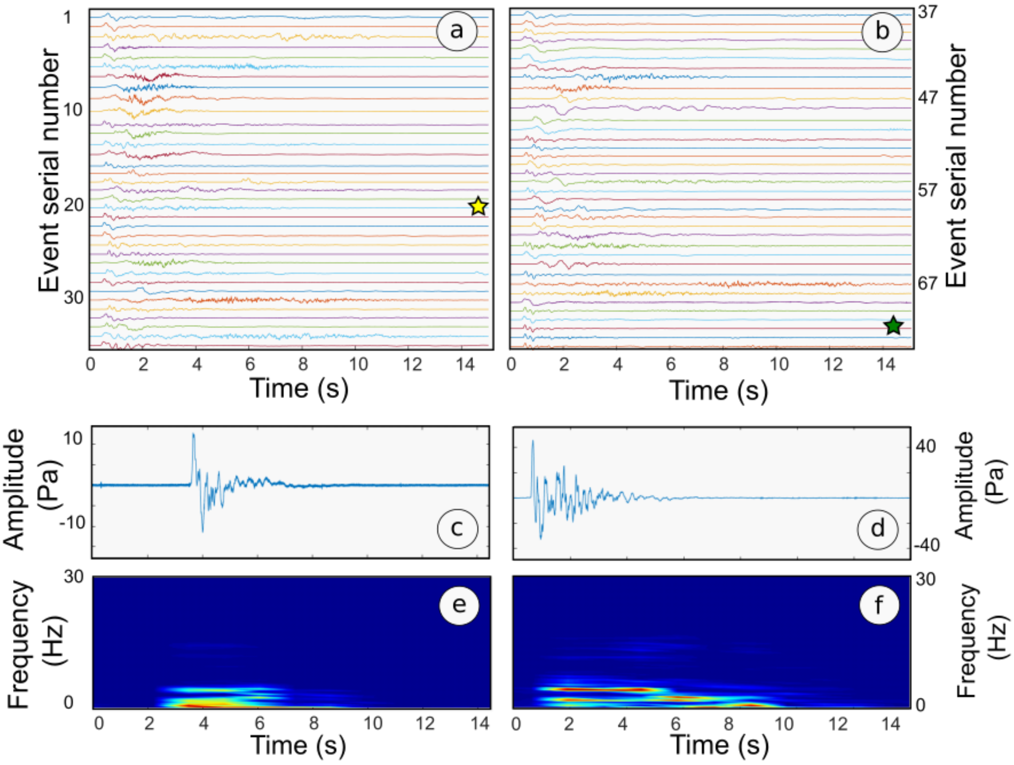

Figure 3: (a), (b): Triggered infrasonic pressure waveforms of explosive activity at Batu Tara. The events marked by a yellow and a green star are shown in (c) and (d), respectively. (e), (f) show the STFT of (c) and (d), respectively.

The damping properties of the acoustic events were evaluated by Sompi Method (Kumazawa et al. 1990). The Sompi method is based on an autoregressive model, and assumes the signal can be de-convolved in a linear combination of coherent oscillations, i.e. wave elements, with decaying amplitudes plus Gaussian white noise. The quality factor is defined as $Q=-f/2g$, with f and g corresponding to the frequency and growth rate (growth rate of the wave element amplitude), respectively (Kumazawa et al. 1990). A higher quality factor corresponds to slower amplitude decay of the investigated events. We found that an autoregressive order of 16 was producing the best results, and was therefore chosen for our analysis.

Successively, we attempted a classification of acoustic waveforms in different families by correlating their spectra, as previously proposed by Milluzzo et al. (2010) building on Green and Neuberg (2006). To this extent we applied the following steps: 1) A window of 15 seconds of signal was selected and a Butterworth filter in the range 0.5-5 Hz was applied;2) the spectra of these windows were calculated; 3) a cross-correlation matrix was obtained by comparing the spectra using cross-correlation; 4) the spectrum exhibiting the highest number of cross-correlation coefficient above the threshold of 0.9 was selected as master spectrum; 5) the spectra of those events that have cross-correlation coefficient above the above-mentioned threshold were stacked to obtain an average spectrum; 6) the latter was cross-correlated with the original dataset, and all the spectra with a cross-correlation coefficient greater than the threshold were grouped into a family. Then steps 4-6 were repeated for the remaining dataset of events.

The acoustic energy radiated during the explosion was evaluated as follows (e.g. Johnson and Aster, 2005):

$$Ea = 2\pi r^2 \rho_{atm}^{-1} c_{atm}^{-1} \int_{T1}^{T2} \Delta P(t)^2 dt \qquad (3)$$

Where T1 and T2 are the initial and final times of the acoustic signal, r is the distance between the vent and the microphone (1226 m), ρ_{atm} is the air density assumed to be equal to 1.2 kg/m^3 and c_{atm} is the sound speed, corresponding to 340 m/s. It has to be noted that equation (3) might represent an underestimation of the actual acoustic energy within the conduit, due to topographical effects and to the impedance contrast at the vent. Indeed, Lacanna and Ripepe (2020) investigated by 3D finite-difference time-domain analysis the effects of plane-to-spherical acoustic wave conversion in the conduit, assuming volcanic conduit behaves as a classical duct system. The amplitude and radiation patterns outside the duct are controlled by the acoustic impedance at the open end, which is a function of vent radius and pressure wavelength; as a result, at the vent-atmosphere interface a large part of the energy is reflected back to the conduit.

The temporal rate of acoustic energy, i.e. acoustic power, has been broadly used in literature to retrieve information on the flow velocity at the source (e.g. Woulff and McGetchin, 1976; Ripepe et al 2013). Building on the source model theory, the relationship between the amplitude of the first positive infrasonic peak and the exit velocity of the gas at the vent for a monopole (3), dipole (4) and quadrupole (5) source (e.g. De Angelis et al. 2019 for details) has been shaped as follows (Vergniolle and Caplan-Auerbach,2006; Delle Donne and Ripepe, 2012 Ripepe et al., 2013):

$$< p > = \frac{\rho_{atm} R \sqrt{K_d}}{r} v_e^2 \quad \ldots\ldots \quad (4)$$

$$< p > = \frac{\rho_{atm} R \sqrt{K_d}}{r c_{atm}} v_e^3 \quad (5)$$

$$< p > = \frac{\rho_{atm} R \sqrt{K_d}}{r {c_{atm}}^2} v_e^4 \ldots\ldots (6)$$

Where K_d is an empirical constant equal to 1, 10^{-2}, 10^{-5} for a monopole, dipole and quadrupole sources respectively (e.g. Vergniolle and Caplan-Auerbach, 2006) and R is the radius of the source. Equations (4) to (6) have been used here to evaluate the gas/particle exit velocity at the vent, assuming different possible source models. The radius of the source has been estimated assuming it is equivalent to half of the average length of the jet at the source (i.e. 6.5 m; see **Section 4.1** for details).

5. Results

5.1 Thermal infrared video results

In the investigated period of data acquisition, explosive events were occurring at a frequency of 2 to 6 events per hour, with the exclusion of a 2-hour interval (5 Sep 7:15 -9:15 UTC) where no events were detected (**Figure 4**). The events recurrence time is between 2 and 36 minutes, with the most frequent intervals being ca. 5 and ca. 12 minutes. There is no obvious correlation between recurrence interval and explosion thermal amplitude during the time span considered.

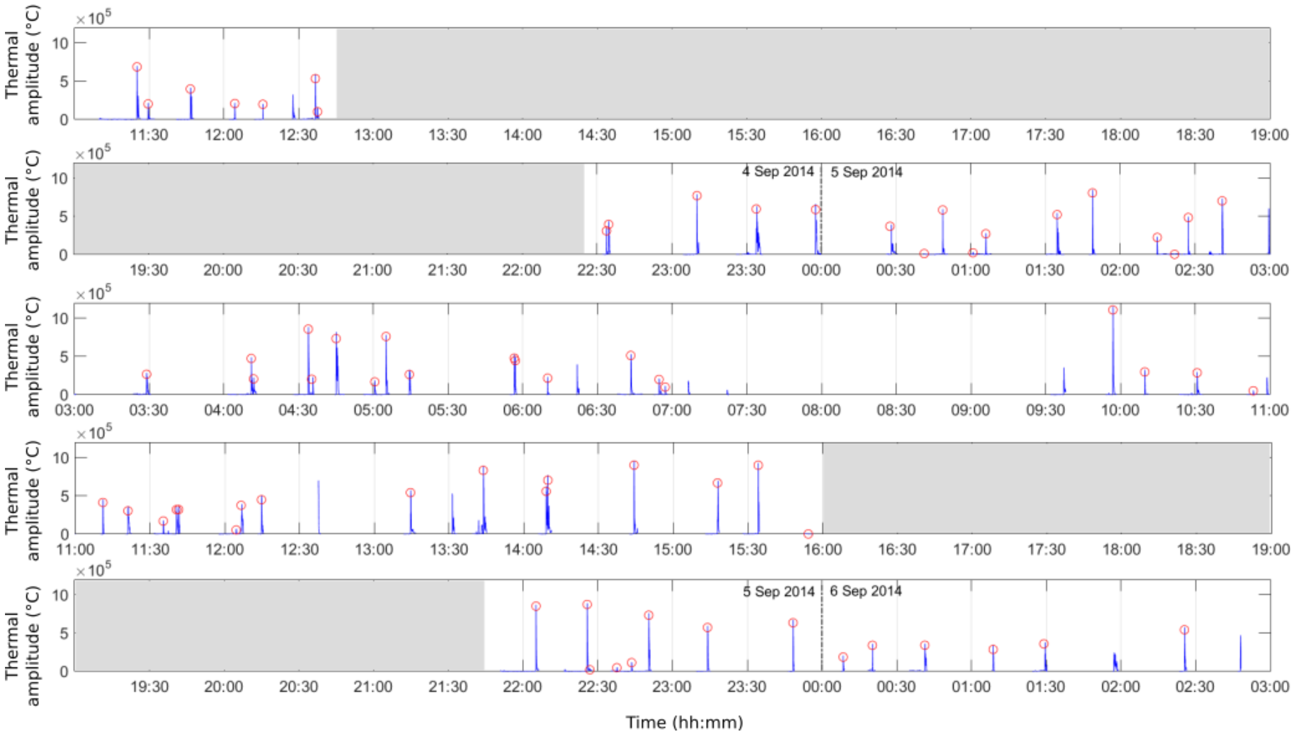

Figure 4: Time series of the triggered thermal events. Each event is displayed as a vertical blue line. The red circles indicate the position of the thermal amplitude peak of the event detected with the STA/LTA algorithm. Grey boxes mark time intervals where no video/audio-recordings are available. Dotted black lines highlight different days.

Thermal waveforms show a unimodal distribution in terms of event duration ranging 2 to 60 seconds, with more than 60% of the events ranging in the 10-30 s interval, and a broad unimodal distribution of amplitudes centred around 2-4x10^5 K. Event thermal energy ranges between 1.1x10^9 and 2.2x10^{11} J, with a bimodal distribution (major peak at 2x10^{10} J and secondary peak at 5x10^9 J). No obvious correlation is observed between peak amplitude and duration (**Figure 5a-c**). The ejection velocity of the bombs and plumes was retrieved from the time/height diagrams of the maximum temperature. Nearly half of the events (33 out of 67) are characterised by one individual bomb ejection pulse, 19 events have two main pulses, whereas the rest show 3 or more ejection pulses. Bomb velocity ranged in the 10-50 m/s with a mode around 20-30 m/s, whereas plumes were ejected at lower velocities (5-25 m/s) with a mode at 6-9 m/s. Maximum bomb elevation widely ranged from 50 to larger than 300 m, exceeding the limit of vertical FOV in ca 20% of the events. Ash and gas plumes can be detected up to 200 -300 m in 90 % of the cases, above that height they become thermally transparent (**Figure 5d-e**). We note a correlation between bomb content, discriminated by visual inspection, and bomb velocity (**Figure 5f**), bomb-rich explosions displaying the highest values (30-50 m/s, with 2 events up to 100 m/s), and ash-dominated ones showing the lowest values (10-20 m/s). We manually tracked a few particles exiting the vent during three selected explosive events using high-speed videos and retrieved speeds in the range 92-331 m/s (04/09, 23:10), 220-460 m/s (05/09, 00:25) and 100-500 m/s (05/09, 00:40), respectively. Such values of velocity are in line with values measured at Stromboli and Yasur (Vanuatu) (e.g. Taddeucci et al. 2012, Spina et al.,2016b), and are representative of the highly accelerated portion of the jet at the vent exit. Velocity values measured from the thermal infrared videos are significantly lower because of the lower spatial and temporal resolution of the FLIR thermal camera compared to high-speed one and to the fact that our thermally derived velocities are retrieved from the slope of the bomb's trajectories (**Figure 2**) and thus are to be considered as representing an average velocity of the bomb from the exit position to its maximum elevation.

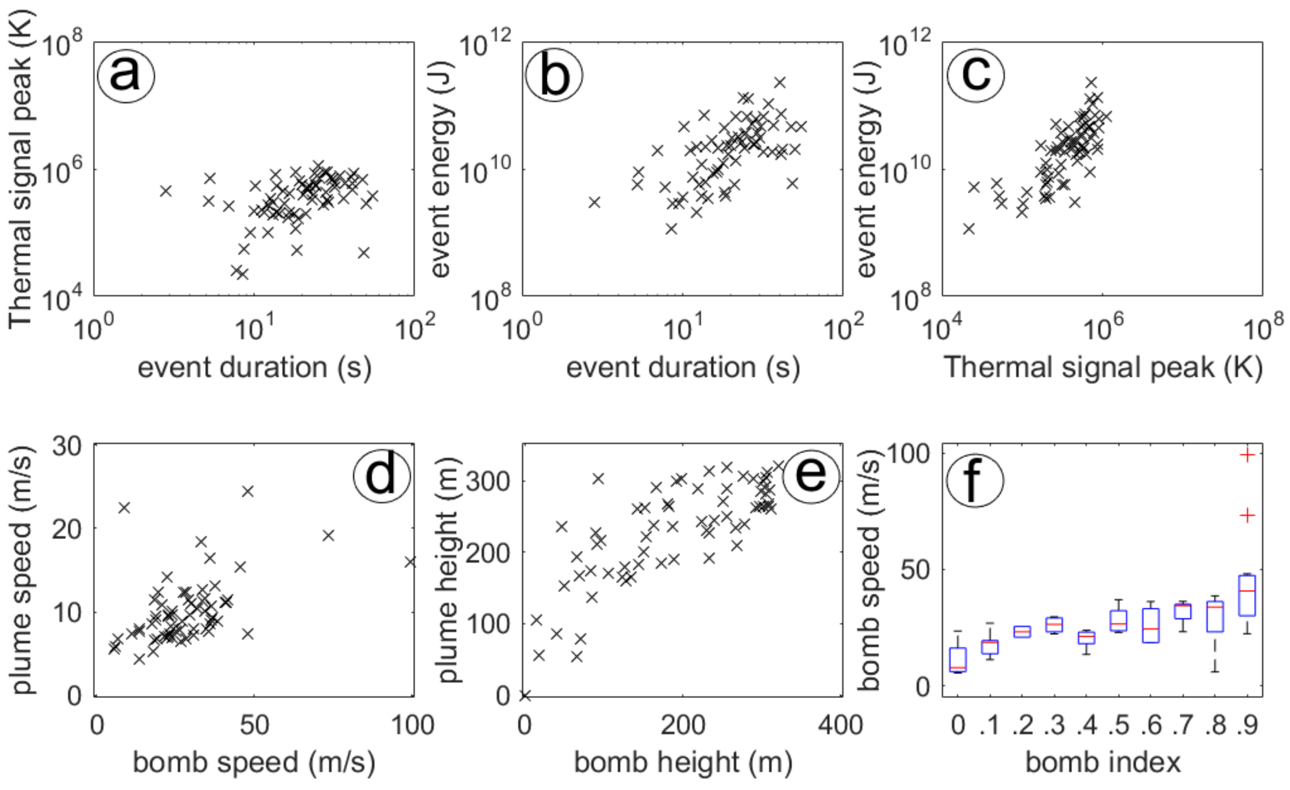

Figure 5: Duration of the event plotted against amplitude of the thermal waveform peak (a) and (b) thermally radiated energy. (c) Amplitude of the thermal waveform peak against thermal energy; bomb vs plume speed (d) and height (e) as computed from time vs height plot of the thermal anomaly (see text); (f) correlation between bomb velocity and bomb index, reflecting purely ash, bomb-free (=0) vs bomb-rich (=1) explosive events.

4.2 Acoustic signals results

The 72 acoustic signals are characterized by discrete transients, mostly exhibiting a compressive impulsive onset followed by a nearly symmetrical rarefaction peak and by a differently developed coda. These are occasionally related to secondary pulses (confirmed by thermal and high-speed images), as also frequently recognized for other volcanoes (De Angelis et al., 2019). Waveforms variability (**Figure 3a** and **3b**) reflects on the widespread distribution of event durations, spanning 2-22 seconds (**Supplementary Figure 1a**). The peak-to-peak amplitude of the events lies mostly in the range 0-100 Pa; three exceptional high-amplitude events with peak-to-peak amplitude of ca. 184, 272, and 384 Pa lasting around one-tenth of second were observed (**Supplementary Figure 1b**).

The peak frequency of the acoustic events mostly lies below 1 Hz (**Supplementary Figure 1d**), whilst mean frequency can reach values up to 15 Hz, with a mean value of 3.5±3, suggesting a relatively broadband spectrum at least for some of the events (**Supplementary Figure 1e**). The quality factor spans over two orders of magnitude (0.33 up to 50), although it is mostly clustered below 10 (**Supplementary Figure 1f**). Acoustic energy lies mostly in the range 10^4-10^9 J, with few exceptions as low as 10^2J (**Supplementary Figure 1g**).

The exit velocity of gas at the vent has been computed by using equations (4), (5), and (6), assuming different radiation patterns. For a monopole source ranges between 5 and 165 m/s with an average value of 38 m/s. Dipole sources correspond to exit velocity of 44-450 m/s (average 160 m/s) whereas a quadrupole source implies exit velocities between 176 and 999 m/s with an average of 450 m/s.

Spectra cross-correlation successfully classified 54 events (up to 75% of the dataset) in six families. Family I, II, and IV gather the highest number of events. All three families include mostly dichromatic spectra (**Figure**

6a, b, and **d**), but with different partitioning of spectral energies among the two peaks. In particular, Family I displays the greatest variability of the dataset and is characterized by the first spectral peak falling in the range 0.66-1.6 Hz and overpowering the higher frequency peak (4.3-4.6 Hz). Family II exhibits relatively higher spectral content on the second peak, at ca. 4.6 Hz compared to the Family I, but the low-frequency peak (0.99-1.6 Hz) still remains dominant in terms of energy. Family IV exhibit an almost perfectly dichromatic spectrum, mostly peaked at 1.6 Hz and 4.6-4.9 Hz. Family III and V are monochromatic and exhibit very low spectral peaks (ca. 0.7-0.99 Hz; **Figure 6c** and **e**). Finally, Family VI has a relative tendency to a broad-band distribution of the spectral energy (**Figure 6f**).

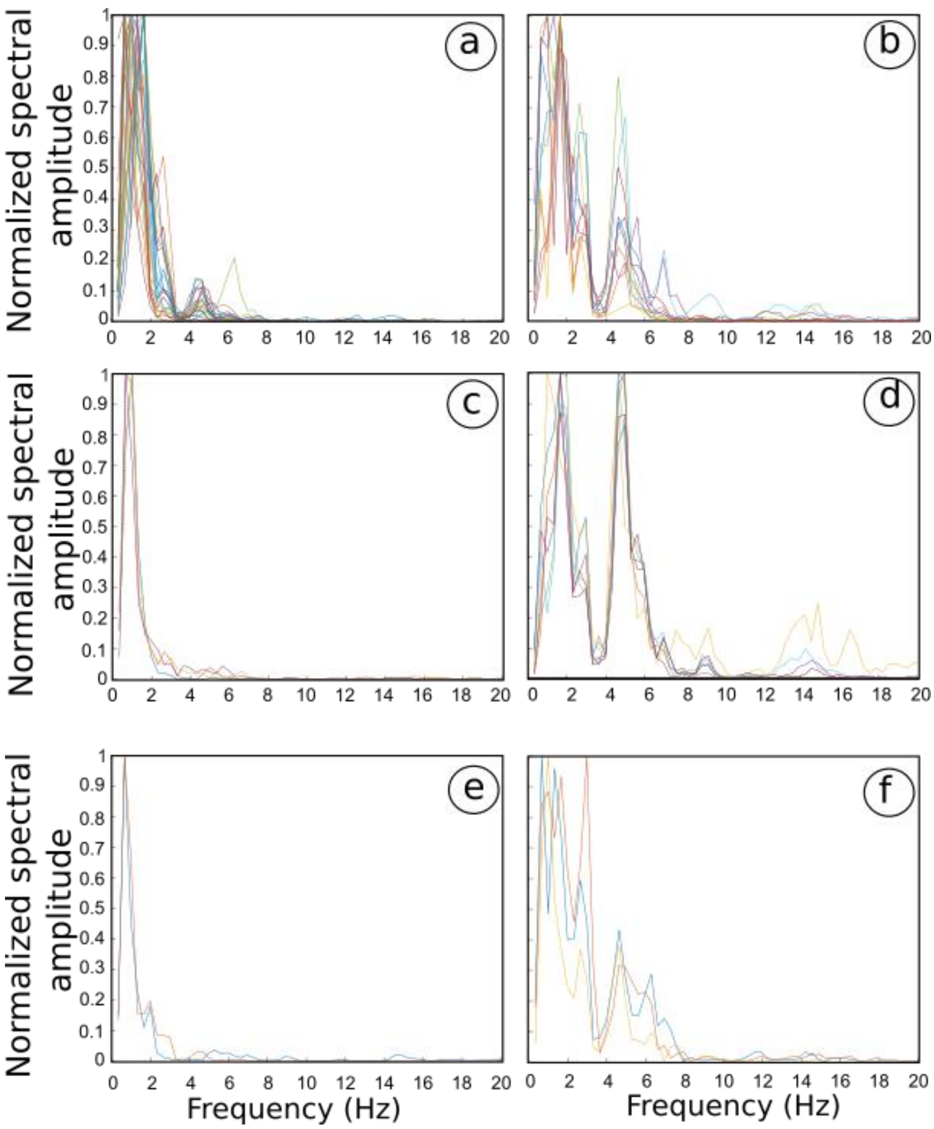

Figure 6 (a) to (e) Overlapped normalized frequency spectra of the family I-VI.

5. Discussion

5.1 Eruption dynamics at Batu Tara

In the studied period, the correlation among the investigated parameters characterizing acoustic or thermal transients revealed that the duration of the acoustic events tends to be positively correlated with the height of the ash plume (**Figure 7a**): events lasting longer than 10 seconds exhibit plume height above 180 meters. This evidence suggests that longer acoustic events correspond to longer source emission. It is worth noting that thermally detected durations are, on average, from 1.2 to 2 times higher than acoustically detected ones. Acoustic duration does not scale with the peak-to-peak amplitude of the events (**Figure 7b**; longer events are not necessarily characterized by stronger overpressure, oppositely to the observation of Matoza et al. 2014). Interestingly, comparison to the bomb index suggests that high-amplitude events are related to bomb-dominated explosions (**Figure 7c**). This observation also matches with the evidence that bomb-dominated explosions display higher velocities of the bombs (**Figure 5f**) pointing to the evidence that bomb-dominated explosions have more explosive energy than ash-dominated ones. Coherently, at Yasur volcano (Vanuatu) a progressive shift from bomb-rich explosion to ash-rich ones has been linked to progressive volatile reduction and/or increase in magma viscosity (Simons et al. 2020). Finally, with only one exception, acoustic events with Quality factors above 10 (**Figure 7d**), exhibit mean frequencies above 5 Hz. This suggests that broadband-spectrum-events are related to source processes exhibiting low rates of energy losses.

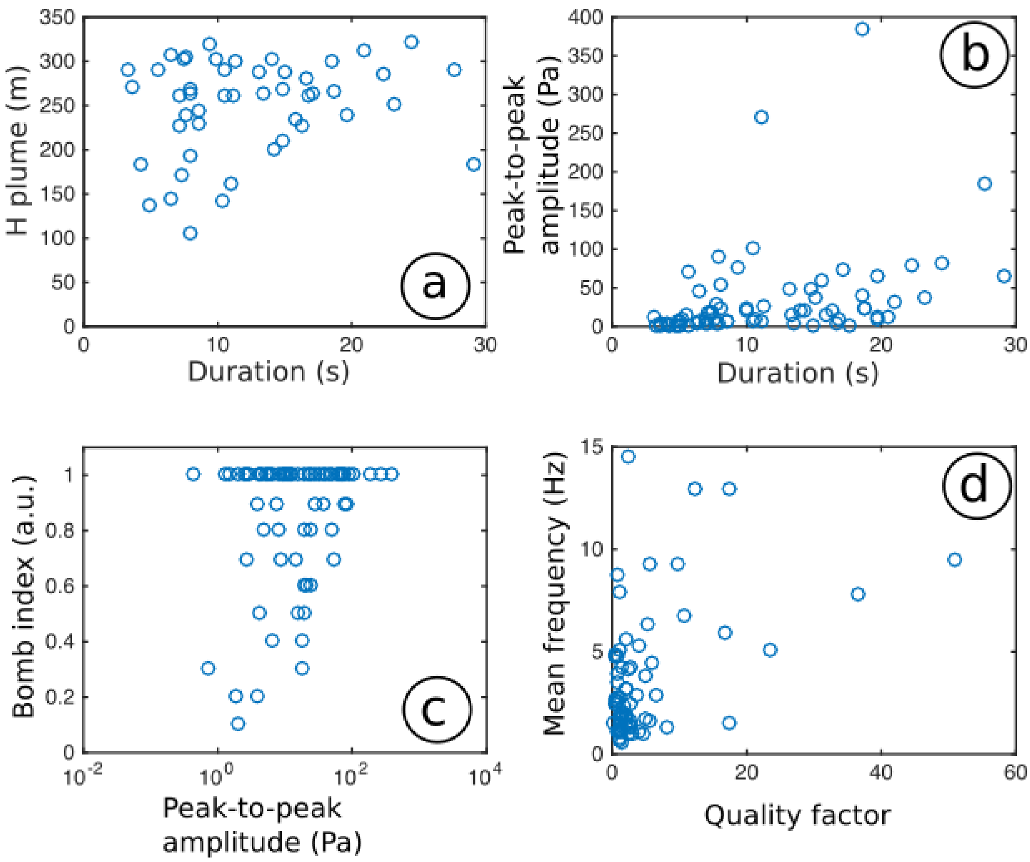

Figure 7: Comparison among different investigated parameters. In (a) and (b) the duration of the acoustic events is plotted against the height of the erupted plume and the peak-to-peak amplitude of the acoustic events, respectively. In (c) the latter is charted together with the bomb index, that provides a qualitative evaluation of the bomb content in the eruptive plume. In (d) the quality factor of the acoustic events computed by Sompi method is plotted against the mean frequency.

Exit velocities of particles at the vent computed from high-speed images fall within the range of 90-500 m/s. This range of values nicely fits gas exit velocities computed for dipole sources (54-464 m/s) that could in fact represent a reasonable choice for short-lived (few tens of seconds) explosive events associated with plumes rising up to their highest elevation within few minutes (De Angelis et al., 2019), despite their inherent uncertainties. Indeed, exit velocities computed following equation (4) to (6) suffer from limits in the assumption and in the spatial sampling of data, as reported in several studies (e. g., Matoza et al., 2013 and De Angelis et al., 2019. For instance: 1) waveform inversion demonstrated that the most realistic source models are a combination of monopole (as the injection of mass in the atmosphere) and dipole sources (Johnson et al. 2008) or eventually even higher-order source term (including quadrupole sources when, for instance, turbulence is dominant) when dealing with sustained eruptions; 2) Matoza et al. (2013) observed that in the absence of good spatial sampling of jet noise directionality, that is in practice usually not possible in volcano acoustic field experiments, the power evaluated might not be representative of the source; 3) the derivation of gas exit velocity from equation (3) neglects the effects of topography and attenuation, factors that have been often demonstrated to be a relevant contribution (De Angelis et al. 2019). Consequently, cross-validation with thermal imagery, here performed, is strongly recommended (De Angelis et al., 2019).

The different families of acoustic events identified by spectra cross-correlation can address differences in the geometry of the plumbing system (e.g. Johnson et al. 2018). The analysis of the identified acoustic families suggests that the acoustic source of Batu Tara explosive events correspond to an open-closed pipe resonance of the upper conduit. Noteworthy, pipe resonance associated with the dipole streamline of the acoustic sound field have been postulated (Rayleigh, 1945; Elder, 1992; Chanaud, 2010).

Pipe resonance of the volcanic system has been widely documented at different volcanoes worldwide, providing several information on the geometry of the feeding system (e.g. Garces and McNutt, 1997; Jhonson et al. 2018; Yokoo et al., 2019; Witsil and Johnson, 2018; Watson et al. 2020). Watson et al. (2019) investigated the effects of volcanic crater geometries, temperature profiles, gas compositions, and source descriptions on infrasound by a linearized model of quasi one-dimensional (1D) wave propagation inside volcanic crater coupled with 3D axisymmetric radiation into the atmosphere from the crater. They found that crater geometry has a most prominent role compared with temperature and gas composition. A volcanic conduit represents an open-closed pipe resonator open to the atmosphere on one side and having an impedance contrast (e.g., the surface of the magmatic column, the fragmentation level, or a conduit cross-section variation) at the other side. In the case of a flanged open-closed pipe resonator, the fundamental frequency is a function of sound speed (c) and resonator length (L) and radius (R_r) as follows (Kinsler et al. 1999):

$$fo = \frac{c}{4(L + \frac{8R_r}{3\pi})}$$

Harmonic frequencies are generated as odd multiples of the fundamental. In our case, a fundamental peak corresponding with the main peak at 1.5-1.6 Hz would have a second harmonic at 4.6-4.9 Hz, in agreement with the second peak we observe. This is evident especially in Family IV (**Figure 6d**) and can be hypothesised also for Family I and II that suffer from a much wider distribution of the fundamental frequency due to a higher number of events gathering in the acoustic families, including lower frequencies events (0.6-0.99 Hz). Hence, Family III and V are likely to represent an end-member low-frequency case where harmonics are missing at all. Indeed, monochromatic acoustic infrasound waves have been described and related to conduit pipe resonance at Aso Volcano (Yokoo et al. 2019). For a fundamental frequency in the range 0.6-1.6, assuming a conduit radius equal to 6.5, the length of the conduit resonating span from a minimum value of almost 50 m (assuming c equal to 340 m/s and f0 corresponding to 1.6 Hz) up to a maximum of ca. 290 m (assuming c equal to 700 m/s, equal to that of magmatic gases at eruptive temperature; Weill et al. 1992), and f0 corresponding to 0.6 Hz).

The different partitioning of spectral energy among different peaks that motivate family classification can be tentatively explained in analogy with musical instruments such as clarinet, i.e. an open-closed pipe resonator. Computer-based studies addressing the behaviour of a clarinet demonstrated that for the same note (same fundamental and duration) the spectral centroid (i.e. a sort of centre of mass of the spectrum) moves toward higher frequencies with increasing mouth pressure or reed opening (Barthet et al. 2007). We can speculate therefore that differences in the input source triggering the conduit resonance or in the conduit geometry (e.g. flaring), resulting from the erosion or accumulation of products within the vent, are likely to produce the different partition of acoustic energy in the spectra of the sorted families. The latter hypothesis is justified by the evidence of coupling between volcanic flow and conduit shape in time and depth (e.g. Macedonio et al. 1994), that is known to affect seismic and acoustic signals (Johnson et al., 2018, Spina et al., 2019), and also by the evidence that the presence of a debris clog or a vent plug can increase the explosivity of the eruption (Del Bello et al., 2015; Capponi et al., 2016).

5.2 Strombolian or Vulcanian explosions

The acoustic amplitudes and durations measured at Batu Tara are comparable to Vulcanian explosions observed at Popocatepetl (Mexico) (e.g. Aràmbula-Mendoza et al., 2013), to violent Strombolian activity at Yasur (Vanuatu) (e.g. Marchetti et al. 2013), to the so called ash-explosions at Karymsky (Russia) (Lopez et al., 2013) and partly to vulcanian explosion at Sakurajima (Japan) (Johnson and Miller, 2014) volcanoes. Explosion duration and mean bomb velocity/height fall well in the range displayed by small Strombolian activity at Etna, Yasur, and Stromboli (Bombrun et al., 2016; Gaudin et al., 2017), despite more frequently observed values of durations at Batu Tara are on the high-end member. Acoustic energy, spanning 10^2-10^9 J, overlaps the range found by Marchetti et al. (2009) for Fuego, Stromboli, Villarica and Santiaguito volcanoes (10^1-10^8) as closely resembling also values provided for Strombolian eruptions at Aso, Yasur, and Arenal (10^4-10^8) by Zobin et al. (2019). Thermal energies, spanning 3 orders of magnitude, (10^9 - 10^{11}) show minimal overlap and are mostly higher than the values for Strombolian to Fire-fountaining activity at Mt. Etna (10^6-10^9, Bombrun et al. 2016), and those for Stromboli, Villarica, Santiaguito and Fuego volcanoes (10^5-10^9, Marchetti et al., 2009). This is consistent with the general longer thermal duration of the events of Batu Tara compared to Santiaguito, Fuego, and Etna volcanoes, reflecting higher thermal radiation energy values, but cannot be the only factor. According to Marchetti et al. (2009), infrasonic energy reflects the contribution of the gas-thrust phase of the explosion, i.e. the release of over-pressurized gas, whereas thermal radiation energy mostly accounts for the whole explosion dynamics, including the buoyant ascent phase, i.e. the floating ascent of the jet/plume into the atmosphere. In the case of Batu Tara, despite acoustic energies are very similar to those at Stromboli and Fuego (**Figure 8**), thermal radiation energy exhibits higher values. A dominance of buoyancy processes (as expected when thermal energies are much higher than infrasonic energies) has been related by Marchetti et al. (2009) to the efficiency of fragmentation processes, i.e. to the amount of ash in the explosive jet. Investigated explosions of Batu Tara are all ash-rich, as opposed to those of Stromboli and Fuego, that are more frequently emitting coarsely-fragmented ejecta. Therefore, embracing the same simplifying assumptions as in Marchetti et al. (2009), we assume that despite the amount of gas over-pressure generating Batu-Tara explosions may be similar to Stromboli and Fuego explosive activity, the fragmentation mechanism at Batu Tara could be more efficient, producing higher proportion of fine vs coarse fragments, and thus a different volumetric concentration of the solid fraction in the plume.

Such uncertainty in quantitatively discriminating the eruptive type, i.e. Vulcanian or Strombolian, of Batu Tara explosions result from the complexity of establishing a clear boundary for intermediate terms among the two end-members. Intermediate-intensity ash-rich explosions have been widely investigated in the attempt of defining a quantitative classification scheme, often comparing eruptive activity at the same volcanoes and at different volcanoes worldwide. For instance, Matoza et al. (2014) investigated three datasets of acoustic events from Sakurajima, Karymsky, and Tungurahua volcano, finding an inherent complexity and variability in explosion styles at individual volcanoes, and at the same time, bulk similarities (Matoza et al. 2014). Houghton and Gonnermann (2008) attempted to define novel criteria to identify different eruptive styles at basaltic volcanoes and pointed to the lack of clear correlation between eruptive rate/steadiness and style, whereas the duration of the eruptive event is considered a more distinctive parameter. A recent review of the classification schemes for Strombolian activity, based on thermal images and including events from Stromboli, Yasur, Etna and Batu Tara, revealed commonalities in the eruptions, which formed a continuum spectrum sharing the same controlling factors (Gaudin et al., 2017). Our analysis of the explosive activity at Batu Tara supports, within the limits of the investigated temporal window, this view of a continuum spectrum of activity, with no gap separating events that span one to two orders of magnitude in eruption parameters.

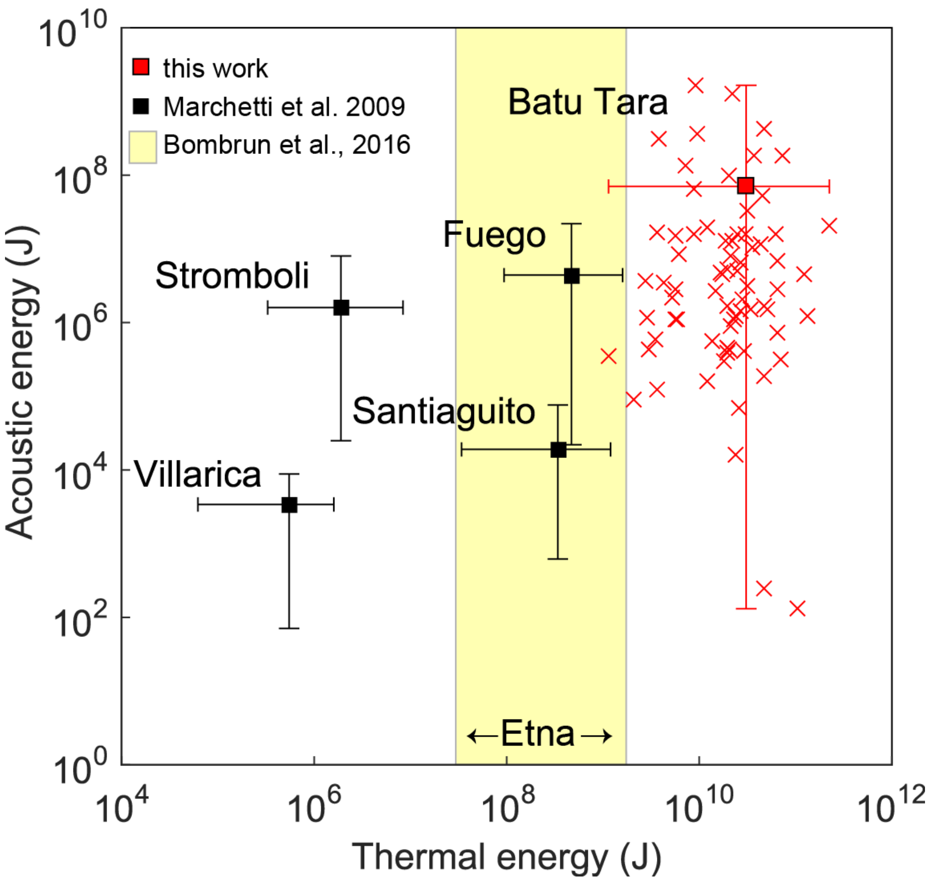

Figure 8: Comparison between acoustic and thermal radiation energy measured at Batu Tara for different explosive events (red crosses) with the acoustic and thermal energies measured at Stromboli, Fuego, Villarica, and Santiaguito (Marchetti et al., 2009), and Etna (thermal energies only, Bombrun et al., 2016).

6. Conclusive remarks

In September 2014 we carried out a multi-parametric campaign aimed at characterizing ongoing explosive activity at Batu Tara Volcano (Flores Sea, Indonesia). The resulting integrated extensive analysis of thermal and acoustic signal from several eruptive events, here described, represent a unique tool for a close-up picture of the eruptive dynamics of a poorly monitored volcano. We summarized the main results in bullet points below:

1) The investigated eruptive activity of Batu Tara Volcano was characterized by intermediate-size bomb-free to bomb-rich ash explosions, with plumes rising few hundred meters above the eruptive vents

with a frequency of ca. 2-6 events per hour. The associated thermal transients, with duration unimodally distributed in the range 2-60 seconds, show energy in the range $1.1x10^9$ and $2.2x10^{11}$ J. The acoustic signal is composed of discrete transients lasting up to a few tens of seconds, featuring a relative waveform variability, acoustic amplitude of ca. 0-300 Pa and energy spanning the range 10^2-10^9 J.

2) Cross-checking observation from the high-speed cameras with the exit velocity computed from source model theory provides a nice fit for a dipole source, and suggests an exit velocity at the vent on the order of 50-500 m/s.

3) The spectral properties of the dataset, that are at the base of the sorting of the acoustic events in different families, suggest that the upper portion of the volcanic conduit may act as an open-closed pipe resonator. For fundamental frequencies in the range 0.66-1.6 and assuming acoustic velocities of 340-700 m/s, the length of the resonating conduit falls in the range to 50-300 m. We speculate that different partitioning among spectral peaks likely reflects variable pressure of the source triggering resonance or different flange of the conduit geometry, possibly due to debris clogging/viscous plugging at the vent.

4) Comparison of the investigated dataset with quantitative information on Strombolian or Vulcanian explosions at other volcanoes support the hypothesis that eruptive activity occurs within a continuum spectrum of activity. Quantitative classification scheme aimed at distinguishing different classes of events often fail due to the inherent complexity of the source processes.

Acknowledgments

We kindly thank M. Patrick and an anonymous reviewer for improving the manuscript. D. Gaudin is acknowledged for creating the original Matlab code used for thermal brightness anomaly retrieval from thermal images. C. Cesaroni is acknowledged for instrument deployment and help in data acquisition at Batu Tara. L.S. wish to thank the “INGV Progetto di Ricerca Libera” Project ROUGHER.

Data availability

The dataset used in this work was collected during field campaign by the authors and may be available upon request to the authors.

References

Arámbula-Mendoza, R., Valdés-González, C., Varley, N., Juárez-García, B., Alonso-Rivera, P., & Hernández-Joffre, V. (2013). Observation of vulcanian explosions with seismic and acoustic data at Popocatépetl volcano, Mexico. Monitoring of Volcanic Activity: Methods and Results, 13-33.

Barthet, M., Kronland-Martinet, R., & Ystad, S. (2007). Improving musical expressiveness by time-varying brightness shaping. In International Symposium on Computer Music Modeling and Retrieval (pp. 313-336). Springer, Berlin, Heidelberg.

Blackett, M. (2015). An initial comparison of the thermal anomaly detection products of MODIS and VIIRS in their observation of Indonesian volcanic activity. Remote Sensing of Environment, volume 171 : 75-82 http://dx.doi.org/10.1016/j.rse.2015.10.002.

Bombrun, M., Spampinato, L., Harris, A., Barra, V., & Caltabiano, T. (2016). On the transition from strombolian to fountaining activity: a thermal energy-based driver. Bulletin of volcanology, 78(2), 15.

Brouwer , M.A., (1940). Geological and Petrological Investigation on Alkalo and Calcalkali Rock of the Islands Adonara, Lomblen and Batoe Tara. In: Geological Expedition of the University of Amsterdam to the Lesser Sunda Islands. Amsterdam 1940, 2, 56-88.

Brown, S.K., Sparks, R.S.J., Mee, K., Vye-Brown, C., Ilyinskaya, E., Jenkins, S.F., & Loughlin, S.C. (2015). Country and regional profiles of volcanic hazard and risk: Indonesia. In: S. Loughlin, S. Sparks, S. Brown, S. Jenkins, & C. Vye-Brown (Eds.), Global Volcanic Hazards and Risk (pp. 411-816). Cambridge: Cambridge University Press, https://doi.org/10.1017/CBO9781316276273.

Capponi, A., Taddeucci, J., Scarlato, P., & Palladino, D. M. (2016). Recycled ejecta modulating Strombolian explosions. Bulletin of Volcanology, 78(2), 13.

Carniel, R., Del Pin, E., Budai, R., & Pascolo, P. (2005). Identifying timescales and possible precursors of the awake to asleep transition in EOG time series. Chaos, Solitons & Fractals, 23(4), 1259-1266.

Chanaud, R. C. (2010). Tools for analyzing sound sources. Essex, CT: CCR Associates, LLC.

Cimarelli, C., Alatorre-Ibargüengoitia, M. A., Aizawa, K., Yokoo, A., Díaz-Marina, A., Iguchi, M., & Dingwell, D. B. (2016). Multiparametric observation of volcanic lightning: Sakurajima Volcano, Japan. Geophysical Research Letters, 43(9), 4221-4228.

Coppola, D., Laiolo, M., Cigolini, C., Delle Donne, D., & Ripepe, M. (2015). Enhanced volcanic hot-spot detection using MODIS IR data: results from the MIROVA system. Geological Society, London, Special Publications, 426(1):181, http://dx.doi.org/10.1144/SP426.5

Coppola, D., Laiolo, M., Cigolini, C., Massimetti, F., Delle Donne, D., Ripepe, M., ... & Cevuard, S. (2019). Thermal remote sensing for global volcano monitoring: Experiences from the MIROVA system. FrEaS, 7, 362.

Dalton, M. P., Waite, G. P., Watson, I. M., & Nadeau, P. A. (2010). Multiparameter quantification of gas release during weak Strombolian eruptions at Pacaya Volcano, Guatemala. Geophysical Research Letters, 37(9).

De Angelis, S., Diaz-Moreno, A., & Zuccarello, L. (2019). Recent developments and applications of acoustic infrasound to monitor volcanic emissions. Remote sensing, 11(11), 1302.

Del Bello, E., Lane, S. J., James, M. R., Llewellin, E. W., Taddeucci, J., Scarlato, P., & Capponi, A. (2015). Viscous plugging can enhance and modulate explosivity of strombolian eruptions. Earth and planetary science letters, 423, 210-218.

Delle Donne, D., Ripepe, M., 2012. High-frame rate thermal imagery of Strombolian explosion: implication of infrasonic source dynamics. J. Geophys. Res. 117,B09206, http://dx.doi.org/10.1029/2011JB008987.

Ebmeier, S., Biggs, J., Poland, M., Pritchard, M., Zoffoli, S., Furtney, M., & Reath, K. (2019). Satellite geodesy for volcano monitoring in the Sentinel-1 and SAR constellation era. In IGARSS 2019-2019 IEEE International Geoscience and Remote Sensing Symposium (pp. 5465-5467). IEEE.

Elder, S. A. (1992). The mechanism of sound production in organ pipes and cavity resonators. Journal of the Acoustical Society of Japan (E), 13(1), 11-23.

Garcés, M. A., & McNutt, S. R. (1997). Theory of the airborne sound field generated in a resonant magma conduit. Journal of volcanology and geothermal research, 78(3-4), 155-178.

Gaudin, D., Taddeucci J., Scarlato P., Del Bello E., Ricci T., Orr T., Houghton B., Harris A., Rao S., & Bucci, A. (2017). Integrating puffing and explosions in a general scheme for Strombolian-style activity. J. Geophys. Res. Solid Earth, 122, doi:10.1002/2016JB013707.

Gordeev, E. I., & Girina, O. A. (2014). Volcanoes and their hazard to aviation. Herald of the Russian Academy of Sciences, 84(1), 1-8.

Green, D. N., & Neuberg, J. (2006). Waveform classification of volcanic low-frequency earthquake swarms and its implication at Soufrière Hills Volcano, Montserrat. Journal of Volcanology and Geothermal Research, 153(1-2), 51-63.

Hamilton, W.B. (1979). Tectonics of the Indonesian region. U.S. Geol. Surv. Prof Pap. 1078, 1-345, https://doi.org/10.3133/pp1078.

Herrin, J.S., & Costa, F. (2015). Recent activity and magmatic processes at Batu Tara. Goldschmidt Conference, Prague.

Hilton, D., & Craig, H. (1989). A helium isotope transect along the Indonesian archipelago. Nature, 342, 906–908, https://doi.org/10.1038/342906a0.

Hoogewerff, J.A., van Bergen, M.J., Vroon, P.Z., Hertogen, J., Wordel, R., Sneyers, A., Nasution, A., Varekamp, J.C., Moens, H.L.E., & Mouchel, D. (1997). U-series, Sr–Nd–Pb isotope and trace-element systematics across an active island arc–continent collision zone: implications for element transfer at the slab–wedge interface. Geochim. Cosmochim. Acta 61, 1057-1072, https://doi.org/10.1016/S0016-7037(97)84621-2.

Houghton, B. F., & Gonnermann, H. M. (2008). Basaltic explosive volcanism: constraints from deposits and models. Geochemistry, 68(2), 117-140.

Johnson, J. B., & Aster, R. C. (2005). Relative partitioning of acoustic and seismic energy during Strombolian eruptions. Journal of Volcanology and Geothermal Research, 148(3-4), 334-354.

Johnson, J., Aster, R., Jones, K. R., Kyle, P., & McIntosh, B. (2008). Acoustic source characterization of impulsive Strombolian eruptions from the Mount Erebus lava lake. Journal of Volcanology and Geothermal Research, 177(3), 673-686.

Johnson, J. B., & Miller, A. J. (2014). Application of the monopole source to quantify explosive flux during vulcanian explosions at Sakurajima Volcano (Japan). Seismological Research Letters, 85(6), 1163-1176.

Johnson, J. B., Ruiz, M. C., Ortiz, H. D., Watson, L. M., Viracucha, G., Ramon, P., & Almeida, M. (2018). Infrasound tornillos produced by volcán cotopaxi's deep crater. Geophysical Research Letters, 45(11), 5436-5444.

Kinsler, L. E., Frey, A. R., Coppens, A. B., & Sanders, J. V. (1999). Fundamentals of acoustics. Fundamentals of Acoustics, 4th Edition, by Lawrence E. Kinsler, Austin R. Frey, Alan B. Coppens, James V. Sanders, pp. 560. ISBN 0-471-84789-5. Wiley-VCH, December 1999., 560.

Kumazawa, M., Imanishi, Y., Fukao, Y., Furumoto, M., & Yamamoto, A. (1990). A theory of spectral analysis based on the characteristic property of a linear dynamic system. Geophysical Journal International, 101(3), 613-630.

Lacanna, G., & Ripepe, M. (2020). Modeling the Acoustic Flux Inside the Magmatic Conduit by 3D-FDTD Simulation. Journal of Geophysical Research: Solid Earth, 125(6), e2019JB018849.

Laiolo, M., Massimetti, F., Cigolini, C., Ripepe, M. & Coppola, D. (2018). Long-term eruptive trends from space-based thermal and SO2 emissions: a comparative analysis of Stromboli, Batu Tara and Tinakula volcanoes. Bull Volcanol 80, 68 (2018). https://doi.org/10.1007/s00445-018-1242-0 .

Lopez, T., Fee, D., Prata, F., & Dehn, J. (2013). Characterization and interpretation of volcanic activity at Karymsky Volcano, Kamchatka, Russia, using observations of infrasound, volcanic emissions, and thermal imagery. Geochemistry, Geophysics, Geosystems, 14(12), 5106-5127.

Macedonio, G., Dobran, F., & Neri, A. (1994). Erosion processes in volcanic conduits and application to the AD 79 eruption of Vesuvius. Earth and planetary science letters, 121(1-2), 137-152.

Matoza, R. S., Fee, D., Neilsen, T. B., Gee, K. L., & Ogden, D. E. (2013). Aeroacoustics of volcanic jets: Acoustic power estimation and jet velocity dependence. Journal of Geophysical Research: Solid Earth, 118(12), 6269-6284.

Matoza, R. S., Fee, D., & López, T. M. (2014). Acoustic characterization of explosion complexity at Sakurajima, Karymsky, and Tungurahua Volcanoes. Seismological Research Letters, 85(6), 1187-1199.

Marchetti, E., Ripepe, M., Harris, A. J. L., & Delle Donne, D. (2009). Tracing the differences between Vulcanian and Strombolian explosions using infrasonic and thermal radiation energy. Earth and Planetary Science Letters, 279(3-4), 273-281.

Marchetti, E., Ripepe, M., Delle Donne, D., Genco, R., Finizola, A., & Garaebiti, E. (2013). Blast waves from violent explosive activity at Yasur Volcano, Vanuatu. Geophysical Research Letters, 40(22), 5838-5843.

Milluzzo, V., Cannata, A., Alparone, S., Gambino, S., Hellweg, M., Montalto, P., ... & Paonita, A. (2010). Tornillos at Vulcano: Clues to the dynamics of the hydrothermal system. Journal of Volcanology and Geothermal Research, 198(3-4), 377-393.

Pallister, J., & McNutt, S. R. (2015). Synthesis of volcano monitoring. In The encyclopedia of volcanoes (pp. 1151-1171). Academic Press.

Paris, R., Switzer, A. D., Belousova, M., Belousov, A., Ontowirjo, B., Whelley, P. L., & Ulvrova, M. (2014). Volcanic tsunami: a review of source mechanisms, past events and hazards in Southeast Asia (Indonesia, Philippines, Papua New Guinea). Natural Hazards, 70(1), 447-470.

Paris, R. (2015). Source mechanisms of volcanic tsunamis. Philosophical Transactions of the Royal Society A: Mathematical, Physical and Engineering Sciences, 373(2053), 20140380.

Prata, F., & Rose, B. (2015). Volcanic ash hazards to aviation. In The Encyclopedia of Volcanoes (pp. 911-934). Academic Press.

Pyle, D. M., Mather, T. A., & Biggs, J. (2013). Remote sensing of volcanoes and volcanic processes: integrating observation and modelling–introduction. Geological Society, London, Special Publications, 380(1), 1-13.

Ramsey, M. S., & Harris, A. J. (2013). Volcanology 2020: How will thermal remote sensing of volcanic surface activity evolve over the next decade?. Journal of Volcanology and Geothermal research, 249, 217-233.

Rayleigh Lord (J. W. S. Strutt), The Theory of Sound (Dover, New York, 1945), Vol. 2, Chap. 21

Ripepe, M., Bonadonna, C., Folch, A., Delle Donne, D., Lacanna, G., Marchetti, E., & Höskuldsson, A. (2013). Ash-plume dynamics and eruption source parameters by infrasound and thermal imagery: The 2010 Eyjafjallajökull eruption. Earth and Planetary Science Letters, 366, 112-121.

Sonnabend, H.R., (2007). Airlines, Aircrafts and Volcanic Ash, World Meterological Association (WMO) Fourth International Workshop on Volcanic Ash, Rotorua, New Zealand, 26-30 March 2007, report number VAWS/4 WP/07-04.

Simons, B. C., Jolly, A. D., Eccles, J. D., & Cronin, S. J. (2020). Spatiotemporal Relationships between Two Closely-spaced Strombolian-style Vents, Yasur, Vanuatu. Geophysical Research Letters, 47(5), e2019GL085687.

Spina, L., Scheu, B., Cimarelli, C., Arciniega-Ceballos, A., & Dingwell, D. B. (2016a). Time scales of foam stability in shallow conduits: Insights from analogue experiments. Geochemistry, Geophysics, Geosystems, 17(10), 4179-4194.

Spina, L., Taddeucci, J., Cannata, A., Gresta, S., Lodato, L., Privitera, E., ... & Palladino, D. M. (2016b). Explosive volcanic activity at Mt. Yasur: a characterization of the acoustic events (9–12th July 2011). Journal of Volcanology and Geothermal Research, 322, 175-183.

Spina, L., Taddeucci, J., Cannata, A., Sciotto, M., Del Bello, E., Scarlato, P., ... & Pena-Fernandez, J. (2017). Time-series analysis of fissure-fed multi-vent activity: a snapshot from the July 2014 eruption of Etna volcano (Italy). Bulletin of Volcanology, 79(7), 51.

Spina, L., Cannata, A., Morgavi, D., & Perugini, D. (2019). Degassing behaviour at basaltic volcanoes: New insights from experimental investigations of different conduit geometry and magma viscosity. Earth-science reviews, 192, 317-336.

Stolz, A. J., Varne, R., Davies, G. R., Wheller, G. E., Foden, J. D. & Abott, M. J. (1988). The geochemistry and petrogenesis of K-rich alkaline volcanics from the Batu Tara volcano, eastern Sunda arc. Contributions to Mineralogy and Petrology 98, 374-389.

Taddeucci, J., Scarlato, P., Capponi, A., Del Bello, E., Cimarelli, C., Palladino, D. M., & Kueppers, U. (2012). High-speed imaging of strombolian explosions: The ejection velocity of pyroclasts. Geophysical research letters, 39(2).

Taddeucci, J., Alatorre-Ibargüengoitia, M. A., Cruz-Vázquez, O., Del Bello, E., Scarlato, P., & Ricci, T. (2017). In-flight dynamics of volcanic ballistic projectiles. Reviews of Geophysics, 55(3), 675-718.

Taddeucci, J., Scarlato, P., Del Bello, E., Spina, L., Ricci, T., Gaudin, D., & Tournigand, P. Y. (2021). The dynamics of explosive mafic eruptions: New insights from multiparametric observations. In Forecasting and Planning for Volcanic Hazards, Risks, and Disasters (pp. 379-411). Elsevier.

Tilling, R. I. (2008). The critical role of volcano monitoring in risk reduction. Advances in Geosciences, European Geosciences Union, 2008, 14, pp.3-11.

van Bergen, M.J., Vroon, P.Z., Varekamp, J.C., & Poorter, R.P.E. (1992). The origin of the potassic rock suite from Batu Tara volcano (East Sunda Arc, Indonesia). Lithos, 28:3-6, 261-282, https://doi.org/10.1016/0024-4937(92)90010-V.

Vergniolle, S., & Caplan-Auerbach, J. (2006). Basaltic thermals and Subplinian plumes: Constraints from acoustic measurements at Shishaldin volcano, Alaska. Bulletin of Volcanology, 68(7-8), 611-630.

Watson, L. M., Dunham, E. M., & Johnson, J. B. (2019). Simulation and inversion of harmonic infrasound from open-vent volcanoes using an efficient quasi-1D crater model. Journal of Volcanology and Geothermal Research, 380, 64-79.

Watson, L. M., Johnson, J. B., Sciotto, M., & Cannata, A. (2020). Changes in Crater Geometry Revealed by Inversion of Harmonic Infrasound Observations: 24 December 2018 Eruption of Mount Etna, Italy. Geophysical Research Letters, 47(19), e2020GL088077.

Weill, A., Brandeis, G., Vergniolle, S., Baudin, F., Bilbille, J., Fèvre, J. F., ... & Hill, X. (1992). Acoustic sounder measurements of the vertical velocity of volcanic jets at Stromboli volcano. Geophysical Research Letters, 19(23), 2357-2360.

Withers, M., Aster, R., Young, C., Beiriger, J., Harris, M., Moore, S., & Trujillo, J. (1998). A comparison of select trigger algorithms for automated global seismic phase and event detection. Bulletin of the Seismological Society of America, 88(1), 95-106.

Witsil, A. J., & Johnson, J. B. (2018). Infrasound explosion and coda signal investigated with joint analysis of video at Mount Erebus, Antarctica. Journal of Volcanology and Geothermal Research, 357, 306-320.

Woulff, G., & McGetchin, T. R. (1976). Acoustic noise from volcanoes: Theory and experiment. Geophysical Journal International, 45(3), 601-616.

Yokoo, A., Ishii, K., Ohkura, T., & Kim, K. (2019). Monochromatic infrasound waves observed during the 2014–2015 eruption of Aso volcano, Japan. Earth, Planets and Space, 71(1), 12.

Zobin, V. M., Battaglia, J., Melson, W., & Sudo, Y. (2019). Two-stage modeling of Strombolian-type eruptions and quantification of the model parameters: Insight from the seismic and acoustic signals. Physics of the Earth and Planetary Interiors, 297, 106318.

Website references list

Badan Geologi Website, URL: *https://vsi.esdm.go.id/index.php/gunungapi/data-dasar-gunungapi/493-pulu-komba-pulu-kambing-ii-pulu-betah* and URL: https://vsi.esdm.go.id/index.php/kegiatan-pvmbg/download-center/doc_download/361-g-batutara, last access on May 29, 2020.

GEBCO Website, URL: https://www.gebco.net/, last access on May 29, 2020.

Global Volcanism Program (GVP) Webisite (Smithsonian Institution National Museum of Natural History), 2007. Report on Batu Tara (Indonesia) (Wunderman, R., ed.). Bulletin of the Global Volcanism Network, 32:12. Smithsonian Institution. https://doi.org/10.5479/si.GVP.BGVN200712-264260 and URL: https://volcano.si.edu/showreport.cfm?doi=10.5479/si.GVP.BGVN200712-264260, last access on May 29, 2020.

Global Volcanism Program (GVP) Website (Smithsonian Institution National Museum of Natural History), URL: https://volcano.si.edu/volcano.cfm?vn=264260 and URL: https://volcano.si.edu/volcano.cfm?vn=264260, last access on May 29, 2020.

Global Volcanism Program (GVP) Website (Smithsonian Institution National Museum of Natural History), 2016. Report on Batu Tara (Indonesia) (Venzke, E., ed.). Bulletin of the Global Volcanism Network, 41:11. Smithsonian Institution. https://doi.org/10.5479/si.GVP.BGVN201611-264260 and URL: https://volcano.si.edu/showreport.cfm?doi=10.5479/si.GVP.BGVN201611-264260, last access on May 29, 2020.

MODIS Website; http://modis.higp.hawaii.edu/, last access on May 20, 2020.

VAAC Darwin Archive, URL: ftp://ftp.bom.gov.au/anon/gen/vaac/, last access on May 29, 2020

Volcano Discovery Website, URL: https://www.volcanodiscovery.com/batu-tara.html and URL: https://www.*volcanodiscovery.com/batu-tara/news/2007/all.html, last access on May 29, 2020.*

Volcano Live website, URL: http://volcanolive.com/tara.html, last access on May 29, 2020

Supplementary material

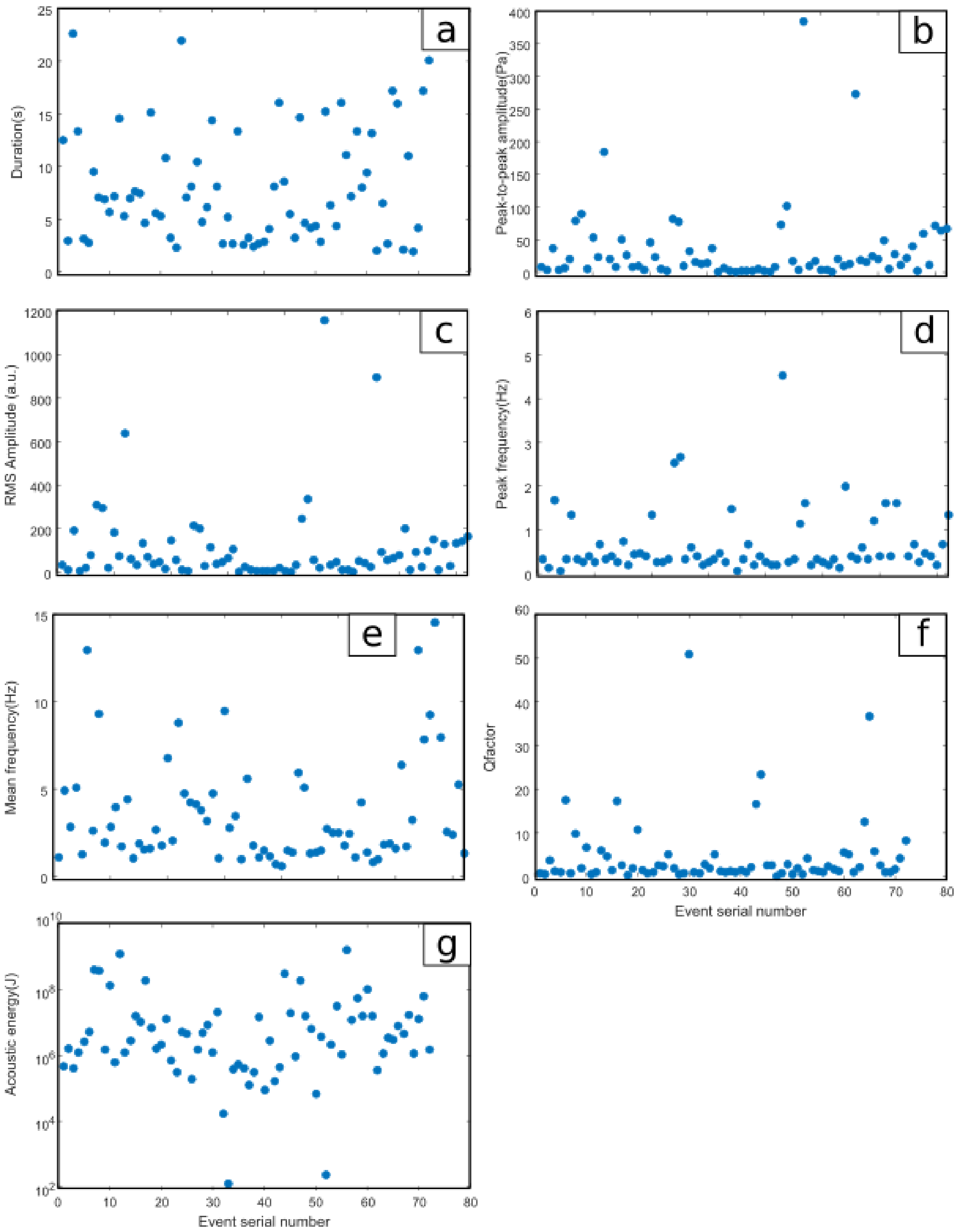

Supplementary Figure 1: Results of different analyses in time and frequency domain of the acoustic events associated with explosive activity from Batu Tara volcano. (a) Duration; (b) Peak-to-peak amplitude, (c) Root-Mean-Square amplitude, (d) Peak frequency, (e) Mean frequency (f) Quality factor, (g) Acoustic Energy.

Supplementary Video 1: Example of two typical explosions detected at Batu Tara.: a bomb-rich explosion (04/09/2014 12:27:34) and a bomb-free one (05/09/2014 12:04:31), recorded in high-frequency mode (200 Hz) with a FLIR thermal camera. The camera FOV is 122x346 m, the real-time duration of the explosion is 4.5 s and 5.9 s, respectively. Some of the largest bombs reach diameters of 5-7 m.

Figure_1

Click here to access/download;Figure;Figure

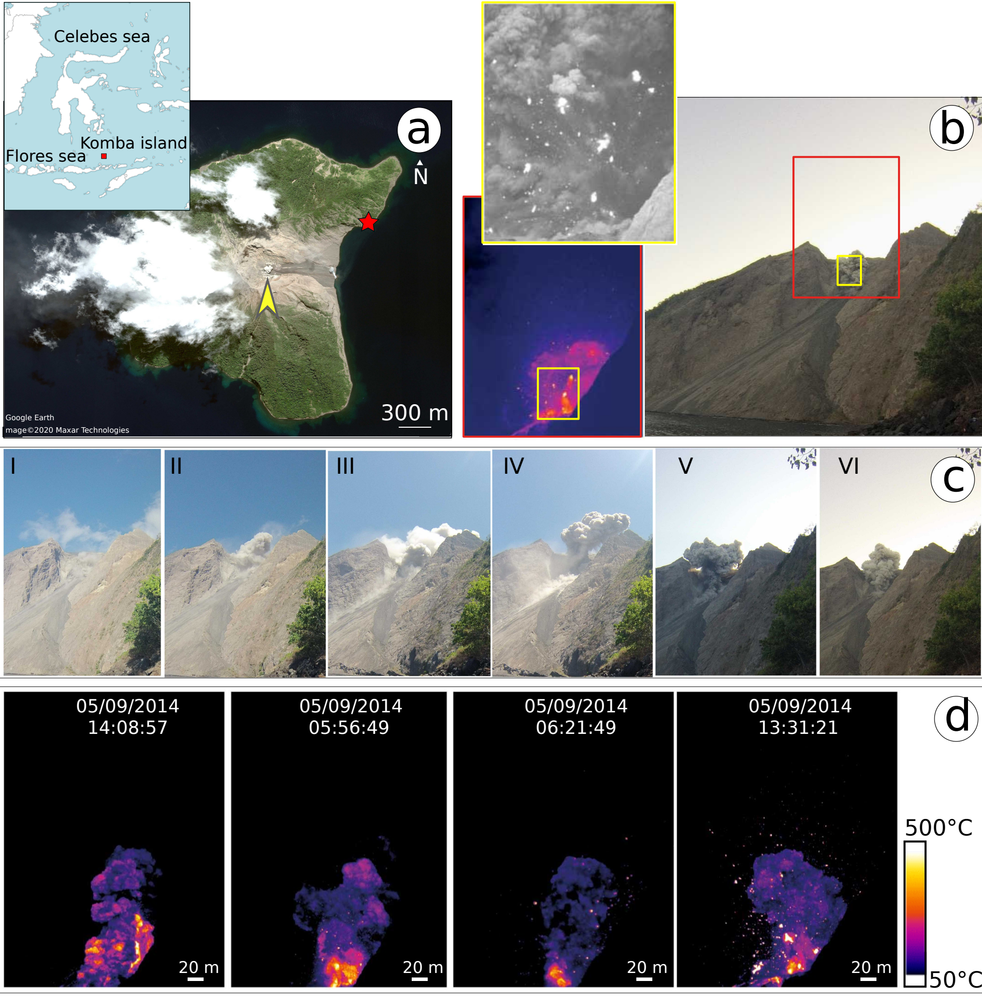

Figure_2

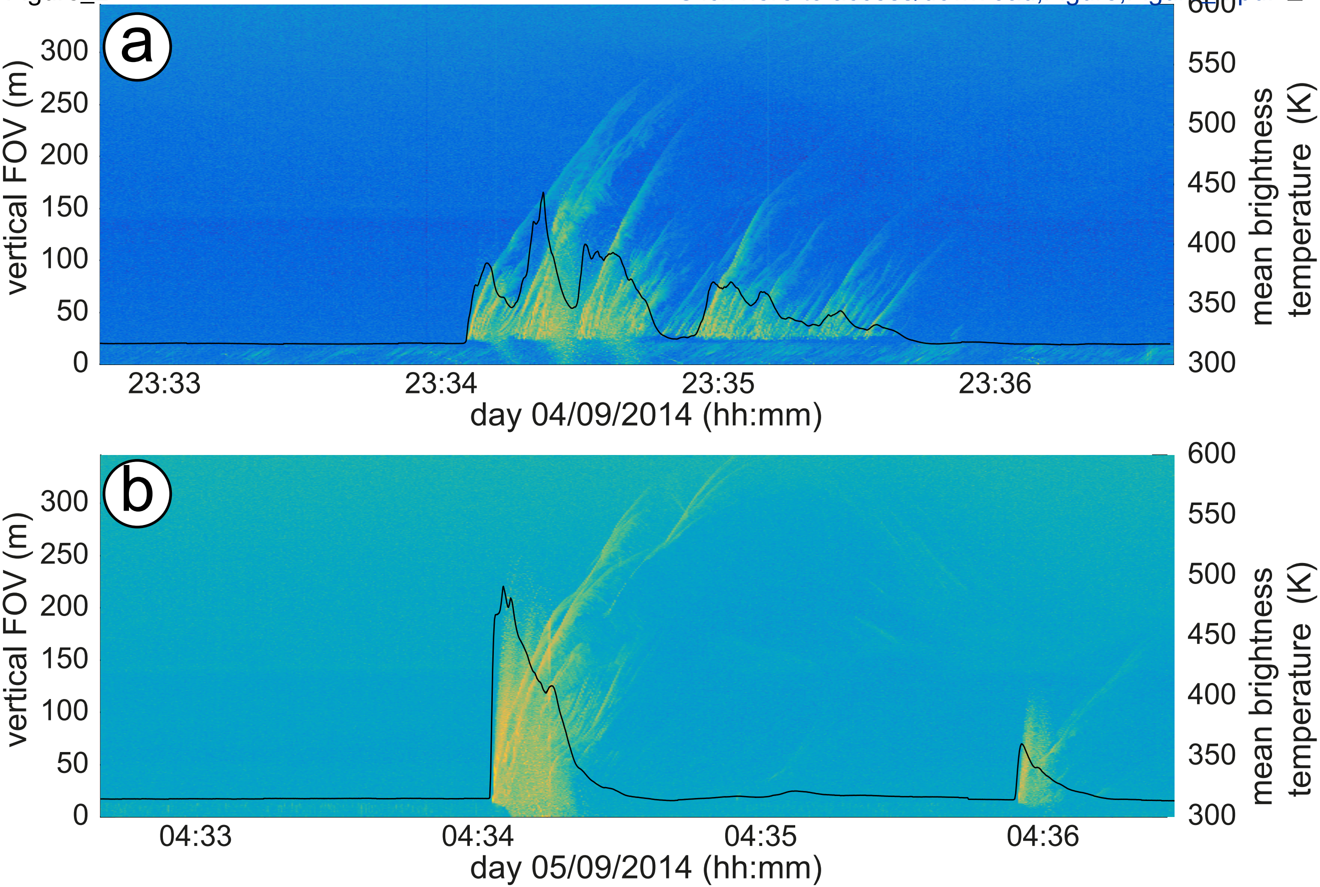
a
vertical FOV (m)
300
250
200
150
100
50
0
mean brightness temperature (K)
600
550
500
450
400
350
300
23:33
23:34
23:35
23:36
day 04/09/2014 (hh:mm)
b
vertical FOV (m)
mean brightness temperature (K)
04:33
04:34
04:35
04:36
day 05/09/2014 (hh:mm)

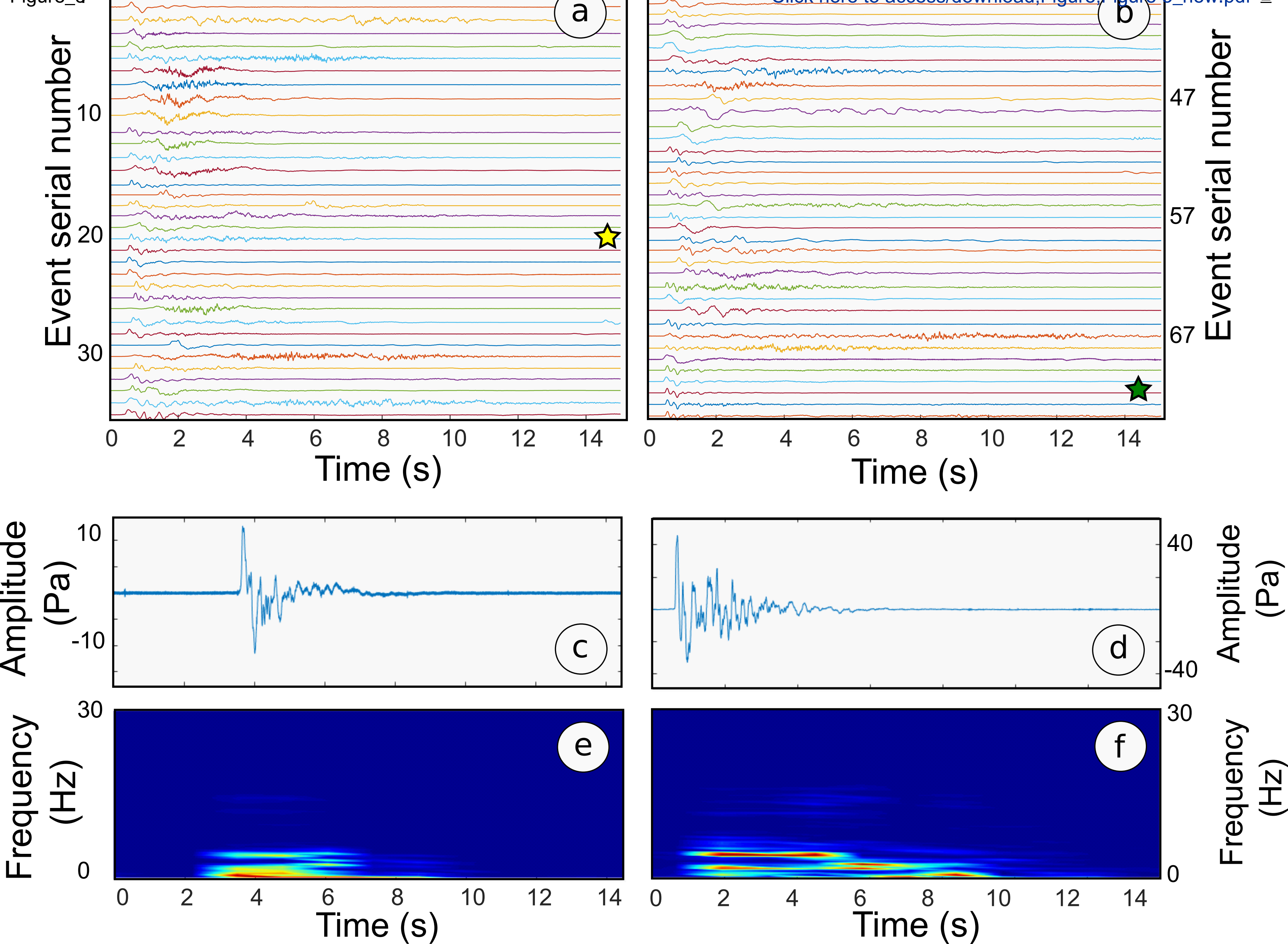
a
b
c
d
e
f
Event serial number
Time (s)
Amplitude (Pa)
Frequency (Hz)
0
2
4
6
8
10
12
14
10
20
30
37
47
57
67
-10
40
-40

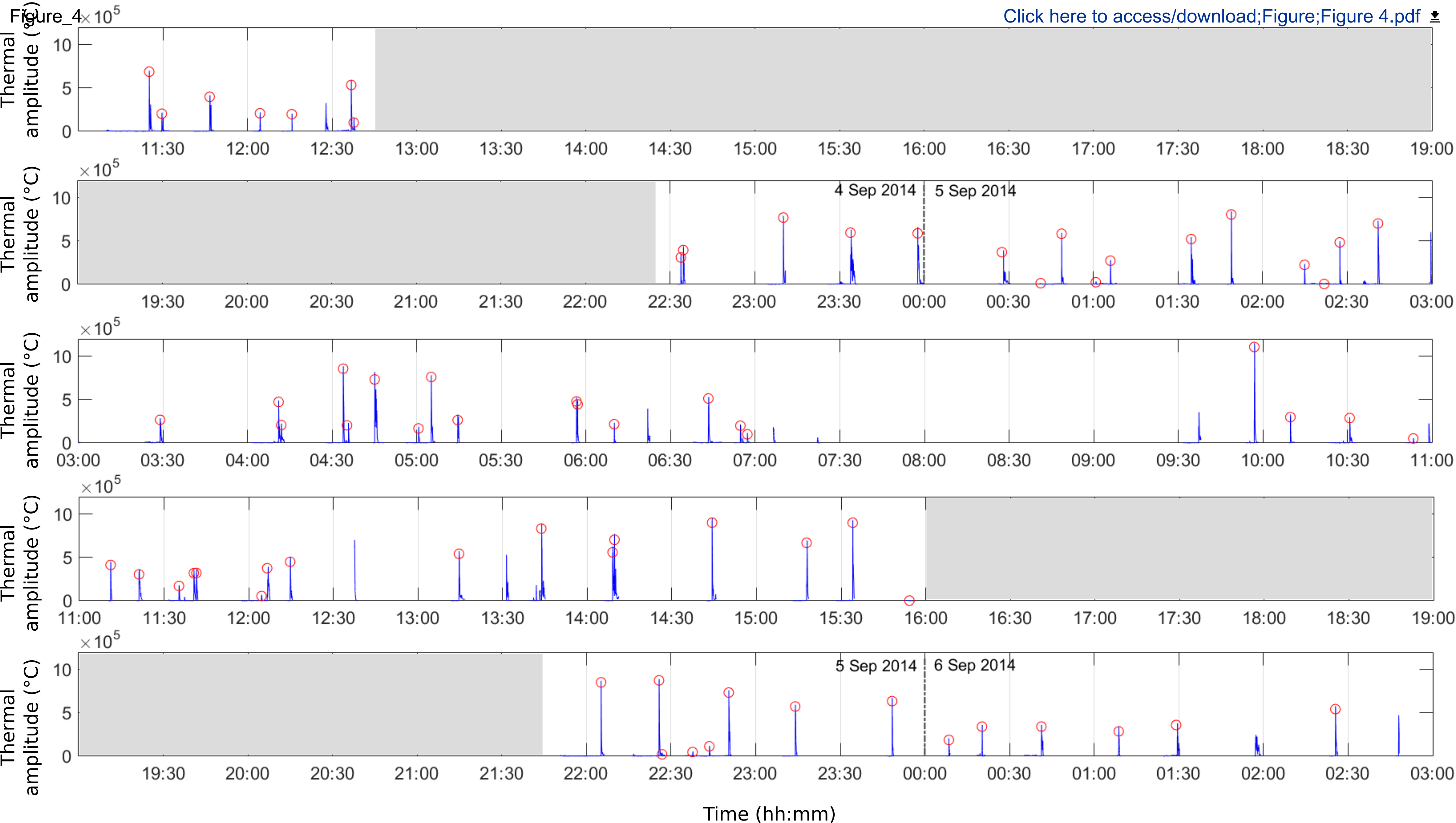
(a)
×10^5
Thermal amplitude (°C)
10
5
0
11:30
12:00
12:30
13:00
13:30
14:00
14:30
15:00
15:30
16:00
16:30
17:00
17:30
18:00
18:30
19:00
19:30
20:00
20:30
21:00
21:30
22:00
22:30
23:00
23:30
00:00
00:30
01:00
01:30
02:00
02:30
03:00
4 Sep 2014
5 Sep 2014
03:00
03:30
04:00
04:30
05:00
05:30
06:00
06:30
07:00
07:30
08:00
08:30
09:00
09:30
10:00
10:30
11:00
11:00
6 Sep 2014
Time (hh:mm)

Figure_5

Click here to access/download;Figure;Figure 5.pdf

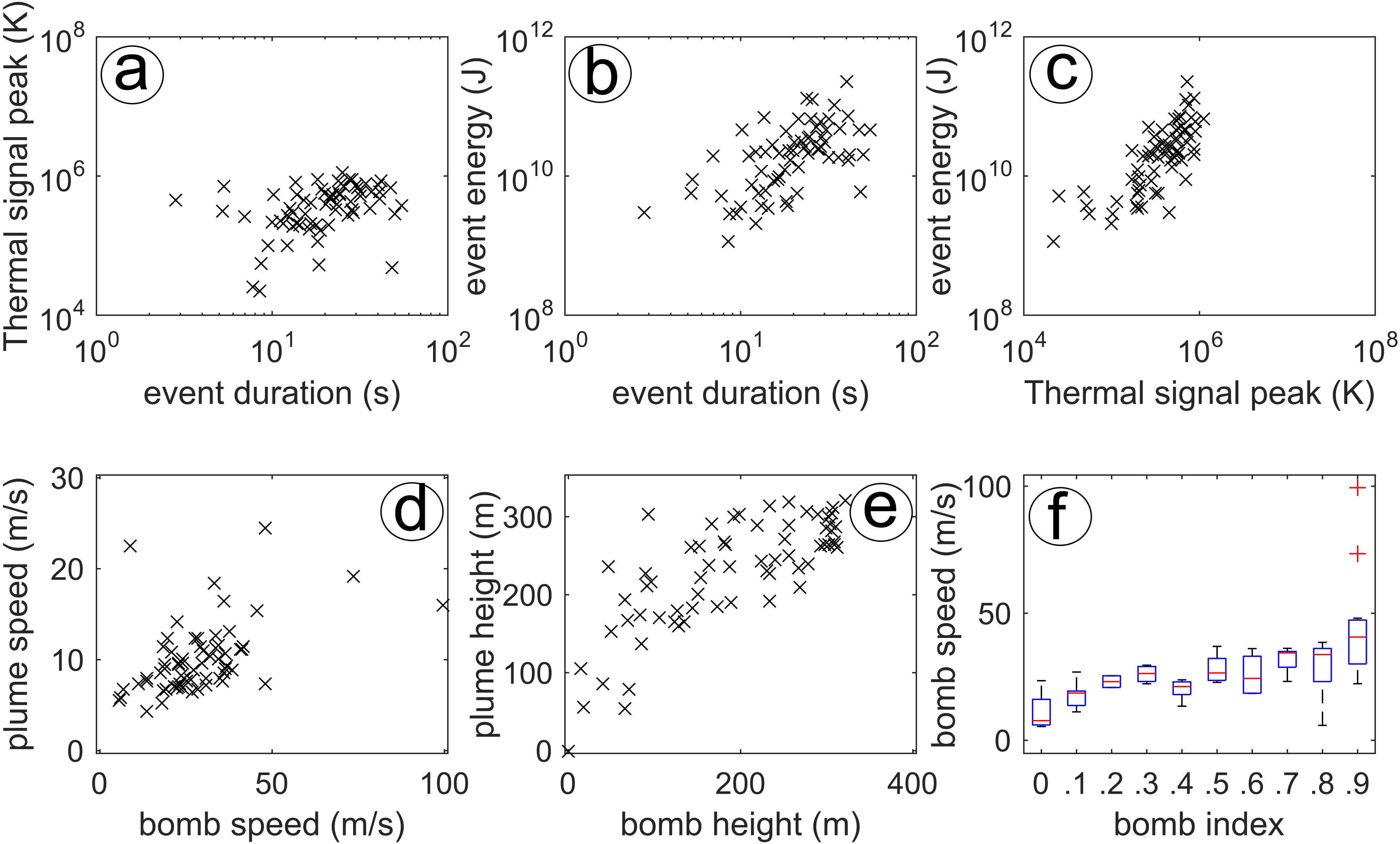

Figure_6

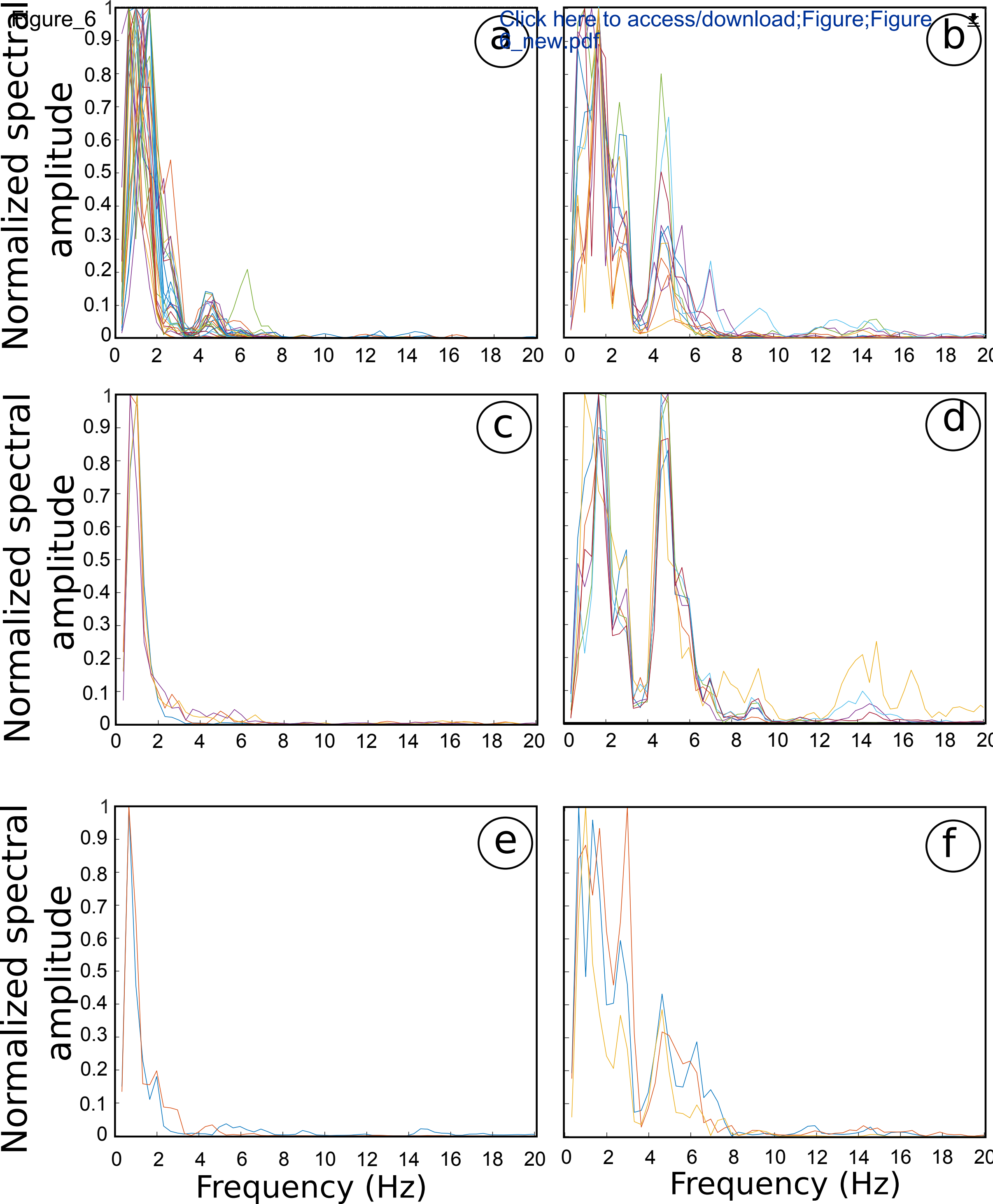
a
b
c
d
e
f
Normalized spectral amplitude
Frequency (Hz)
0
0.1
0.2
0.3
0.4
0.5
0.6
0.7
0.8
0.9
1
0
2
4
6
8
10
12
14
16
18
20

Figure_7

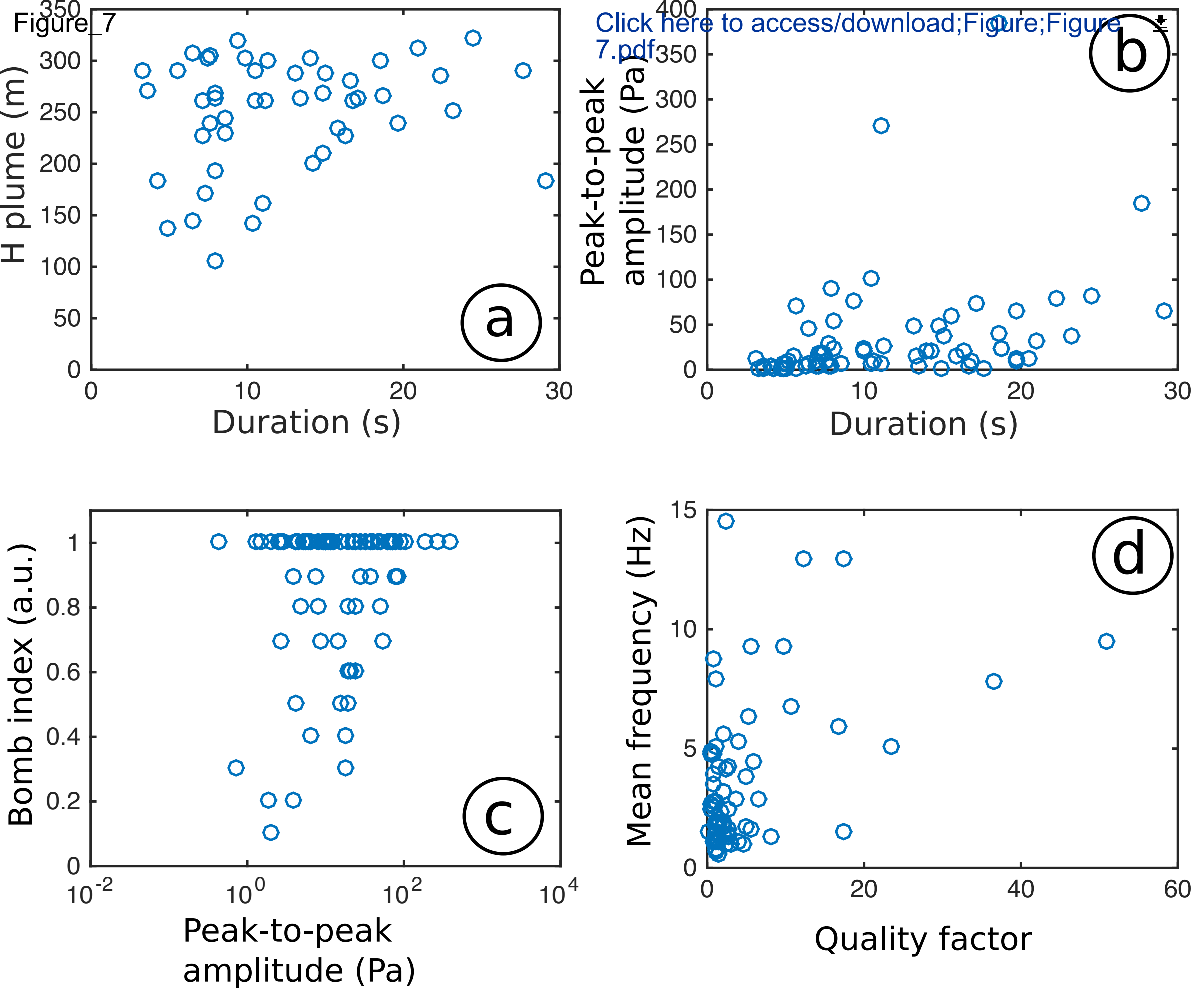

a
H plume (m)
Duration (s)
0
50
100
150
200
250
300
350
0
10
20
30
b
Peak-to-peak amplitude (Pa)
Duration (s)
0
50
100
150
200
250
300
350
400
0
10
20
30
c
Bomb index (a.u.)
Peak-to-peak amplitude (Pa)
0
0.2
0.4
0.6
0.8
1
10^{-2}
10^{0}
10^{2}
10^{4}
d
Mean frequency (Hz)
Quality factor
0
5
10
15
0
20
40
60

Figure_8

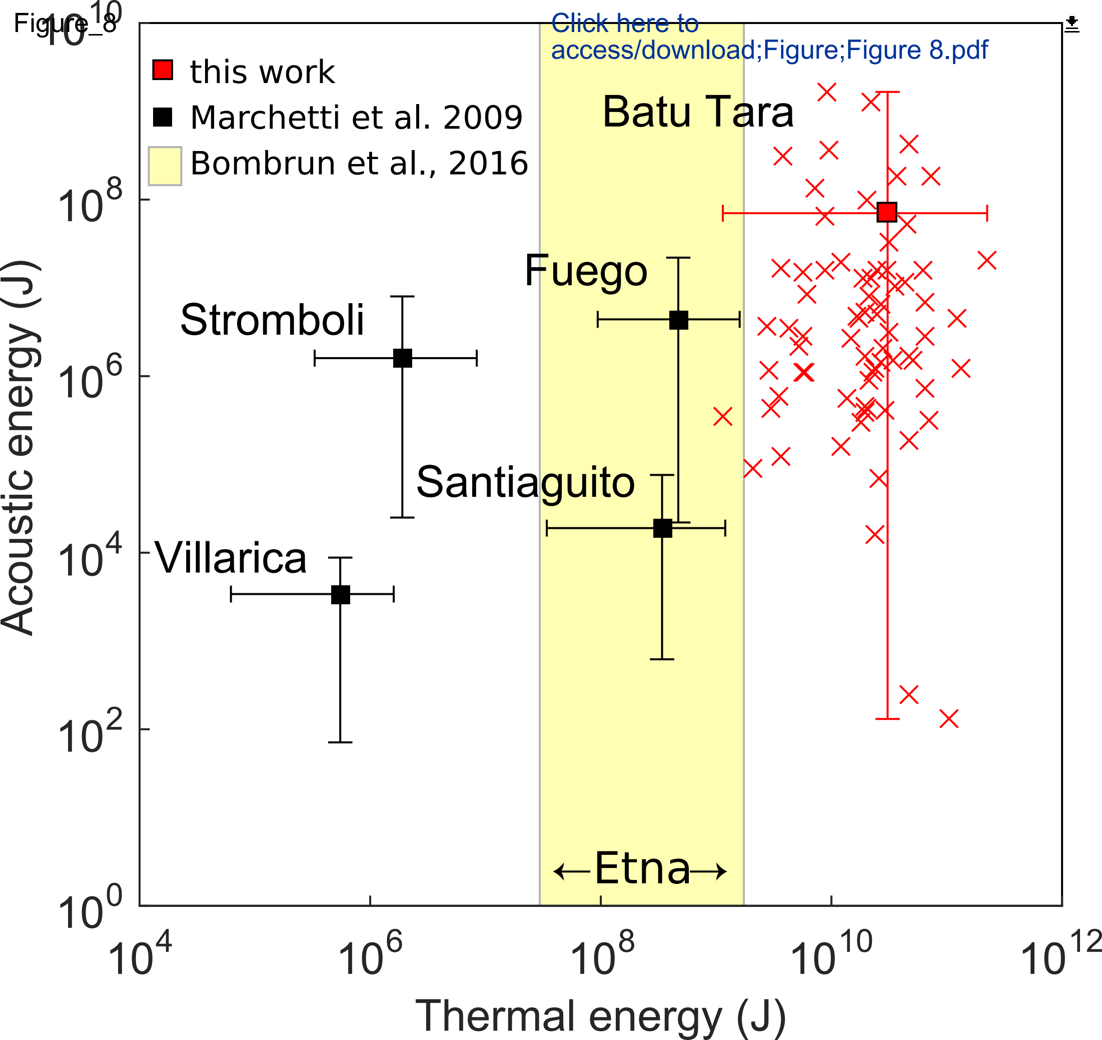
this work
Marchetti et al. 2009
Bombrun et al., 2016
Batu Tara
Fuego
Stromboli
Santiaguito
Villarica
←Etna→
Acoustic energy (J)
Thermal energy (J)
10^{10}
10^{8}
10^{6}
10^{4}
10^{2}
10^{0}
10^{4}
10^{6}
10^{8}
10^{10}
10^{12}

Author statement

L.S. and E.D.B. performed conceptualization, data analysis procedure and article revising. E.D.B., T.R. and P.S. collected data samples. L.S., E.D.B., T.R., J.T and P.S. wrote the paper and contributed to the interpretation of the results.

Supplementary video

Click here to access/download
Supplementary Material
suppl_video.mp4

Supplementary Figure 1

Click here to access/download
Supplementary Material
Supplementary Figure 1.pdf